Article

TRANSPARENT PROCESS OPEN ACCESS

THE EMBO JOURNAL

Nucleosomal arrays self-assemble into supramolecular globular structures lacking 30-nm fibers

Kazuhiro Maeshima[1,2,*,†], Ryan Rogge[3,†], Sachiko Tamura[1], Yasumasa Joti[2,4], Takaaki Hikima[2], Heather Szerlong[3], Christine Krause[3], Jake Herman[3], Erik Seidel[3], Jennifer DeLuca[3], Tetsuya Ishikawa[2] & Jeffrey C Hansen[3,**]

Abstract

The existence of a 30-nm fiber as a basic folding unit for DNA packaging has remained a topic of active discussion. Here, we characterize the supramolecular structures formed by reversible Mg^{2+}-dependent self-association of linear 12-mer nucleosomal arrays using microscopy and physicochemical approaches. These reconstituted chromatin structures, which we call "oligomers", are globular throughout all stages of cooperative assembly and range in size from ~50 nm to a maximum diameter of ~1,000 nm. The nucleosomal arrays were packaged within the oligomers as interdigitated 10-nm fibers, rather than folded 30-nm structures. Linker DNA was freely accessible to micrococcal nuclease, although the oligomers remained partially intact after linker DNA digestion. The organization of chromosomal fibers in human nuclei *in situ* was stabilized by 1 mM $MgCl_2$, but became disrupted in the absence of $MgCl_2$, conditions that also dissociated the oligomers *in vitro*. These results indicate that a 10-nm array of nucleosomes has the intrinsic ability to self-assemble into large chromatin globules stabilized by nucleosome–nucleosome interactions, and suggest that the oligomers are a good *in vitro* model for investigating the structure and organization of interphase chromosomes.

Keywords 10-nm chromatin fiber; analytical ultracentrifugation; microscopy; nucleosomal array; X-ray scattering

Subject Categories Chromatin, Epigenetics, Genomics & Functional Genomics

DOI 10.15252/embj.201592660 | Received 1 August 2015 | Revised 2 February 2016 | Accepted 8 March 2016 | Published online 12 April 2016

The EMBO Journal (2016) 35: 1115–1132

Introduction

In a typical human nucleus, about two meters of DNA is packaged into nucleoprotein structures termed chromatin and then into chromosomes. At its core, a chromosome consists of a single ~50- to 250-Mb DNA molecule assembled into a chain of ~10^5–10^6 nucleosomes. The nucleosome is composed of ~147 bp of DNA bound to an octamer of core histone proteins (H2A, H2B, H3, H4) (Luger *et al*, 1997). Nucleosomes repetitively spaced along DNA at ~160- to 210-bp intervals and connected by stretches of free linker DNA are called nucleosomal arrays (Hansen, 2002). Chromatin refers to nucleosomal arrays bound to linker histone H1 and/or other chromosome-associated proteins. The long linear chromatin molecule is condensed extensively within an interphase chromosome, such that chromosomal DNA can fit inside the nucleus, and during mitosis, the long chromatin chain is further packaged into a mitotic chromosome (Ohta *et al*, 2010; Maeshima *et al*, 2014b; Hirano, 2015).

Physicochemical studies of short nucleosomal arrays, typically 12–60 nucleosomes in length, have shown that chromatin condensation *in vitro* is salt dependent and driven by both intra-fiber and interfiber nucleosome–nucleosome interactions (Hansen, 2002; Pepenella *et al*, 2014). At very low salt concentrations (e.g. < 0.5 mM Mg^{2+}), nucleosomal arrays have an extended beads-on-a-string conformation termed the 10-nm fiber (Hansen, 2002). As salt initially is titrated into solution (e.g. 0.5–2 mM Mg^{2+}), nucleosomal arrays fold into helical structures that are ~30–40 nm in diameter, generically referred to as the "30-nm fiber". Folding is mediated by intra-fiber interactions involving the H4 N-terminal tail domains of one nucleosome with the surface acidic patch domains of neighboring nucleosomes (Luger *et al*, 1997; Kalashnikova *et al*, 2013). Folded 30-nm fibers are stabilized by the H1 linker histones (Hansen, 2002). The structure of the 30-nm fiber has been proposed

1 Biological Macromolecules Laboratory, Structural Biology Center, National Institute of Genetics and Department of Genetics, Sokendai (Graduate University for Advanced Studies), Mishima, Japan
2 RIKEN SPring-8 Center, Sayo-cho, Sayo-gun, Japan
3 Department of Biochemistry and Molecular Biology, Colorado State University, Fort Collins, CO, USA
4 XFEL Utilization Division, Japan Synchrotron Radiation Research Institute (JASRI), Sayo-gun, Japan
*Corresponding author. Tel: +81 55 981 6864; E-mail: kmaeshim@nig.ac.jp
**Corresponding author. Tel: +1 970 491 5440; E-mail: jeffrey.c.hansen@colostate.edu
†These authors contributed equally to this work

to be a one-start solenoid, a two-start zig-zag, or a heteromorphic combination of the two (Robinson & Rhodes, 2006; Grigoryev *et al*, 2009). At higher divalent cation concentrations (e.g. $\geq$ 3 mM Mg^{2+}), short nucleosomal arrays self-associate to form large "oligomers" that pellet immediately in a microfuge (Hansen, 2002). While self-association is mediated by interfiber nucleosome–nucleosome interactions distinct from those involved in folding (Hansen, 2002), nothing is known about the structure, subunit organization, and assembly of the chromatin oligomers due to their extreme size and the lack of available quantitative physicochemical assays.

The widely held paradigm for chromosome structure and assembly holds that the chromosomal fiber first forms a helical 30-nm chromatin structure (Finch & Klug, 1976; Langmore & Paulson, 1983; Woodcock *et al*, 1984; Widom & Klug, 1985; Dorigo *et al*, 2004; Gilbert *et al*, 2004; Schalch *et al*, 2005; Robinson *et al*, 2006; Song *et al*, 2014), mimicking the folding of a nucleosomal array as salt is added into solution. A central premise of this paradigm is that the 30-nm fiber is a requisite folding intermediate in the assembly and maintenance of condensed interphase and mitotic chromosomes. However, small-angle X-ray scattering (SAXS) experiments indicated that no repetitive structures beyond the 10-nm fiber were present in the chromatin of isolated nuclei (Joti *et al*, 2012) or mitotic chromosomes (Nishino *et al*, 2012). Similarly, cryo-electron microscopy (EM) studies of interphase (Bouchet-Marquis *et al*, 2006; Gan *et al*, 2013) and mitotic chromosomes (Eltsov *et al*, 2008), and electron spectroscopic imaging studies of mouse cells (Fussner *et al*, 2012), visualized packed 10-nm fibers, but no folded 30-nm fibers, even in the highly condensed heterochromatin regions. More recent super-resolution imaging also showed heterogeneous groups of nucleosomes called "clutches" (Ricci *et al*, 2015). Based on these results, an alternative model has been proposed in which chromosomes are assembled through long-range interactions of extended 10-nm fibers to form an interdigitated polymer melt-like structure (Maeshima *et al*, 2010, 2014b). In the established paradigm, formation of condensed domains beyond the 30-nm fiber occurs through continuous twisting and coiling of the chromosomal chain of nucleosomes (Alberts *et al*, 2007). Conversely, chromosome conformation capture experiments (e.g. 3C, HiC) suggest that interphase chromosomes are organized into 0.1- to 10-Mb-sized globular structures such as "topologically associating domains" (TADs) (Dixon *et al*, 2012; Nora *et al*, 2012; Sexton *et al*, 2012; Dekker *et al*, 2013; Rao *et al*, 2014; Eagen *et al*, 2015), which further self-associate into discrete chromosomal territories (Cremer & Cremer, 2010). Similarly, globular chromatin domains of ~1 Mb in size have been observed using fluorescence microscopy imaging, as foci of DNA replication via pulse labeling (Albiez *et al*, 2006). Altogether, the new data support a view of chromosome structure and assembly that fundamentally differs from the textbook model. This in turn requires a reexamination of the relationships between chromatin folding and oligomerization *in vitro* and chromosome assembly *in vivo*.

The present studies aim to improve our understanding of chromatin oligomerization and its relevance to chromosome structure and organization. We hypothesize that the fiber–fiber interactions that mediate the oligomerization of short nucleosomal arrays *in vitro* are equivalent to the long-range fiber–fiber interactions that help assemble and organize higher-order chromatin domains within the nucleus. A direct prediction of this hypothesis is that the chromatin oligomers will possess many of the same structural features as an intact interphase chromosome. To test our hypothesis and its predictions, we have used fluorescence light (FM) and transmission electron (TEM) microscopy, sedimentation velocity analytical ultracentrifugation (SV-AUC), and SAXS to quantitatively characterize the structure of the oligomers formed by salt-dependent self-association of 12-mer nucleosomal arrays, and micrococcal nuclease to determine the role of linker DNA in oligomer stability. We also examined the salt dependence of chromatin organization and compaction *in situ*. The *in vitro* studies have yielded novel information regarding the size, morphology, subunit packaging, and mechanism of assembly of the nucleosome oligomers and have revealed the effects of linker histones on the oligomerization transition. The *in vitro* data indicate that the ability to self-assemble through interdigitated packaging of 10-nm fibers into globular structures with diameters of ~50–1,000 nm is an intrinsic property of an array of nucleosomes. In the case of the *in situ* experiments, low salt conditions that disassemble oligomers *in vitro* disrupt heterochromatin and euchromatin compartments and cause extensive chromatin decondensation in isolated nuclei. Collectively, our data support a new paradigm in which long-range interactions of the 10-nm chromatin fiber are important determinants of the structure and organization of interphase chromosomes. Our results further suggest that the chromatin oligomers provide a good *in vitro* model system for investigating eukaryotic chromosome structure and function.

Results

Nucleosomal arrays self-associate into large globular oligomers

The standard assay for nucleosomal array oligomerization is differential centrifugation (Schwarz & Hansen, 1994; Tse & Hansen, 1997). This assay determines the fraction of the chromatin sample that pellets after a short microfuge spin. Figure EV1A shows a control differential centrifugation experiment performed with linear 12-mer 601 (Lowary & Widom, 1998) and 5S (Simpson *et al*, 1985) nucleosomal arrays reconstituted to an average of 11–12 nucleosomes per DNA template. In both cases, all of the nucleosomal arrays in 0–2 mM $MgCl_2$ remained in the supernatant, indicating that no oligomerization had occurred under these conditions. About 10% of the samples pelleted in 3 mM $MgCl_2$, 30% in 4 mM $MgCl_2$, 60% in 4.5 mM, and 90% by 6 mM $MgCl_2$. Altogether, the pelleting curves for the 601 and 5S nucleosomal arrays were superimposable. While these data indicate that both the 601 and 5S nucleosomal arrays formed rapidly sedimenting oligomers in $\geq$ 3 mM $MgCl_2$, this assay yields no structure-based information.

To determine oligomer size and morphology, samples were analyzed by FM and TEM. Representative FM images of the 601 oligomers obtained in 4.5 and 10 mM $MgCl_2$ are shown in Fig 1A. In both salt conditions, the oligomers were globular and had diameters ranging from several hundred to ~1,000 nm. Moreover, the ~1,000-nm particles were the largest oligomers present in 4.5 and 10 mM $MgCl_2$, suggesting that there is an upper size limit to the self-association process. No particles were observed in control images taken at 0–2.5 mM $MgCl_2$ (Fig 1B), consistent with the lack of oligomerization seen by the differential centrifugation assay (Fig EV1A). Of note, the size and morphology of the 5S oligomers

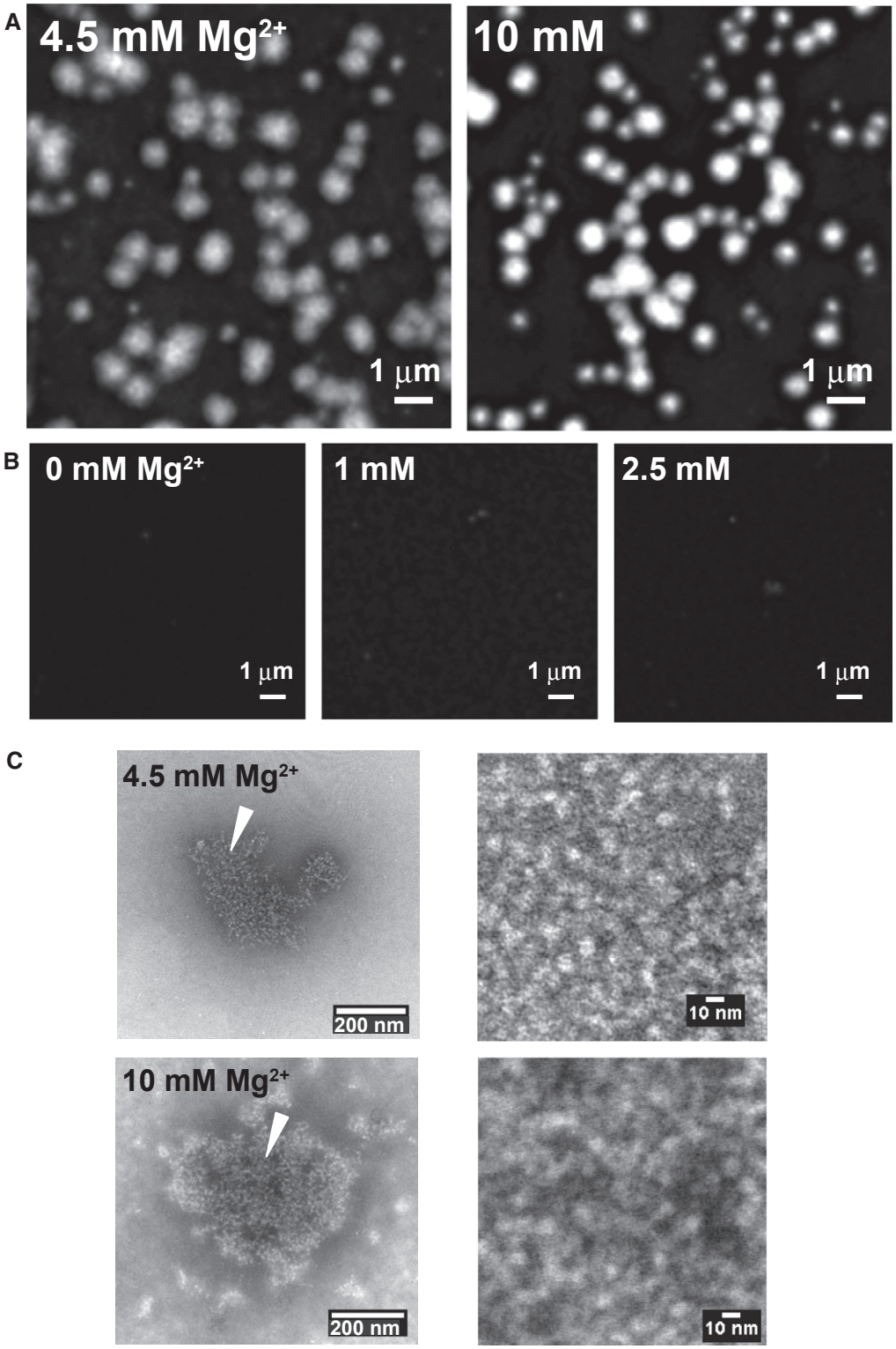

Figure 1. Nucleosomal array oligomers are globular.

A Nucleosomal array oligomers were stained with DAPI and examined using FM (fluorescence microscopy) as described in the Materials and Methods section. Shown are representative images obtained in 4.5 and 10 mM $MgCl_2$.

B Control FM images obtained in 0, 1, and 2.5 mM $MgCl_2$.

C Nucleosomal array oligomers were negatively stained and visualized by TEM as described under Materials and Methods. Shown in the left panels are representative images obtained in 4.5 and 10 mM $MgCl_2$. Shown in the right panels are images of the interior of the oligomers (white arrows, left panels) after cropping and rescaling.

assembled in 5 and 10 mM $MgCl_2$ (Fig EV1B) were similar to those of the 601 oligomers in Fig 1A. Thus, the formation of large globular oligomers was not critically dependent on the nearly perfect nucleosome positioning of the 601 nucleosomal arrays. The 601 oligomers next were characterized by TEM as described by Woodcock *et al* (1991). This protocol involves glutaraldehyde fixation to preserve macromolecular interactions and gross structure, adsorption to a carbon grid, negative staining, and dehydration. Figure 1C shows representative images of the oligomers visualized in 4.5 and 10 mM $MgCl_2$. In both salt conditions, the predominant oligomers observed were globular and ~400 nm in diameter (Fig 1C, left panels), in agreement with the FM results. Darker regions in the TEM images result from pooling of the negative stain, indicating that the surfaces of the oligomers were uneven and textured (Fig 1C, left panels). The edges of the oligomers were irregular, and in some cases, smaller globules could be seen at the periphery of the larger particles (Fig 1C, left panels). At higher magnification, individual nucleosomes could be seen in the interior of the oligomers as bright 10-nm-diameter particles that were closely packed and in physical contact (Fig 1C, right panels). No regular repetitive folded structures such as the 30-nm fiber could be identified at the higher magnifications.

The FM studies (Fig 1) suggest that a population of oligomers exists in solution at any given salt concentration and that the oligomers reach a maximum size of about 1,000 nm in ≥ 4.5 mM $MgCl_2$. An ideal complementary technique to address these questions under native solution conditions and quantitatively characterize macromolecular self-association is SV-AUC (Schuck, 2013). However, in the past, it has not been possible to study oligomerization using SV-AUC and the standard absorption optical system because the oligomers pellet before data can be collected. To overcome this hurdle, we employed the interference optical system, which measures concentration based on refractive properties of the sample and collects a complete concentration versus radial distance dataset in ~2–3 s (compared to about ~90 s for the absorbance optics) (Rogge & Hansen, 2015). The scans obtained from a typical interference SV-AUC experiment in 10 mM $MgCl_2$ are shown in Appendix Fig S1. Under these conditions, the samples formed broad but discrete boundaries during sedimentation, qualitatively indicating that there was a heterogeneous population of oligomers with upper and lower size limits.

To quantitatively analyze the boundaries, we first calculated the weight-averaged second moment sedimentation coefficient (s_{sm}) of the 601 oligomers as a function of $MgCl_2$ (Fig 2A). In 4.0 mM $MgCl_2$ (~30% oligomerized), the s_{sm} was ~30,000S (S, a unit of time equal to 10^{-13} s). The s_{sm} increased to ~100,000S in 4.5 mM $MgCl_2$ (~60% oligomeric) before plateauing at ~200,000S in 5–10 mM $MgCl_2$ (75–100% oligomeric). By comparison, bacteriophage T7 (875S) (Dubin *et al*, 1970) and amyloid fibrils (3,000S) (MacRaild *et al*, 2003) are the largest biological assemblages previously characterized by SV-AUC. Thus, our studies have substantially increased the size threshold for SV-AUC experiments. The plateau in the s_{sm} at ≥ 5 mM $MgCl_2$ was reproducible (Fig 2A, inset). In 4 mM $MgCl_2$, the ~70% of the sample that did not pellet during centrifugation sedimented as monomeric folded 35–45S nucleosomal arrays (Appendix Fig S2). The existence of only nucleosomal array monomers and large oligomers at intermediate extents of self-association demonstrates that oligomerization is highly cooperative. The boundaries of the experiment shown in Fig 2A next were analyzed by

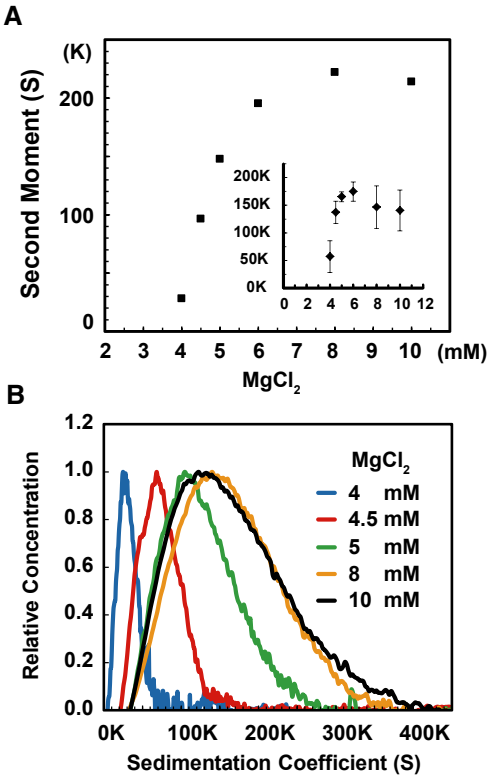

Figure 2. Sedimentation velocity analysis of the salt-dependent assembly of nucleosomal array oligomers.

A Representative experiment showing the second moment sedimentation coefficients of the oligomeric nucleosomal arrays as a function of $MgCl_2$. The second moment sedimentation coefficient is equivalent to the mass average sedimentation coefficient for the entire sample (see Materials and Methods). The inset shows the mean second moment sedimentation coefficient ± the standard error from three replicated experiments.

B Analysis of the same raw data as in (A) by the time-derivative method to yield the sedimentation coefficient distribution, g(s*).

time-derivative method to obtain the distribution of sedimentation coefficient g(s*) (Stafford, 1992). In this analysis, the subsequent scan in a pair of scans is subtracted from the previous scan to determine the change in sample concentration over time. Because the oligomers were extremely large and the sedimentation times very short, the sedimentation coefficient distributions were not expected to be affected by diffusion. In 4.0 mM $MgCl_2$, the sedimentation coefficient distribution of the 601 oligomers ranged from ~5,000 to 60,000S, with a peak in the plot at ~25,000S (Fig 2B). In 4.5 mM $MgCl_2$, the distribution of sedimentation coefficients was shifted to ~25,000–130,000S, and the peak in the g(s*) plot increased to ~70,000S. In 5 mM $MgCl_2$, the 601 oligomers sedimented from ~40,000 to 250,000S, with a peak in the g(s*) plot at ~110,000S. In 8 and 10 mM $MgCl_2$, the g(s*) plots were very similar and yielded sedimentation coefficient distributions from ~40,000 to 350,000S and a peak at ~130,000–140,000S. The overlapping g(s*) plots in 8 and 10 mM $MgCl_2$ (Fig 2B) are consistent with the plateau observed in the s_{sm} versus $MgCl_2$ plot (Fig 2A) and indicate that the 601 oligomers reach a maximum average size of ~140,000S and a maximum absolute size of ~350,000S under ionic conditions that promote

self-association of 100% of the sample. When the 601 nucleosomal arrays were exposed to 8 mM $MgCl_2$ and the sample returned to TE buffer, the oligomers dissociated into a homogeneous population of unfolded ~27–29S monomers (Fig EV2), demonstrating that all steps in Mg^{2+}-induced assembly of the oligomers are reversible (also see Schwarz *et al*, 1996).

The microscopy studies indicate that the oligomers are globular throughout the assembly process. Consequently, a number of physical properties of the oligomers can be calculated from the measured sedimentation coefficients assuming a spherical structure (Table 1). The smallest oligomers detected during the early stages of self-association in 4 mM $MgCl_2$ sedimented at ~5,000S, while the largest oligomers observed in 8 and 10 mM $MgCl_2$ sedimented at ~350,000S. The 5,000S oligomers were estimated to consist of 4.5×10^3 nucleosomes and have a mass of 1×10^9 Da. The Stokes radius, equivalent to the radius of a sphere calculated from the frictional coefficient, was 65 nm and the 5,000S oligomers contained ~1-Mb DNA/oligomer. At the other extreme, the 350,000S oligomers were estimated to have 2×10^6 nucleosomes and a mass of 5×10^{11} Da. The Stokes radius was ~500 nm and the 350,000S particles contained ~450-Mb DNA/oligomer. The estimated Stokes radii are in the range determined by FM and TEM under the same ionic conditions (Fig 1). The calculated mass and Mb DNA/oligomer indicate that the globular oligomers assembled *in vitro* as a function of increasing salt spanned the size range of the chromatin domains found in interphase nuclei (Dixon *et al*, 2012; Nora *et al*, 2012; Sexton *et al*, 2012; Dekker *et al*, 2013; Rao *et al*, 2014; Eagen *et al*, 2015).

Nucleosomal array monomers are packaged as extended 10-nm fibers, not folded 30-nm fibers

An important question is whether the nucleosomal array subunits are packaged within the oligomers as 10- or 30-nm fibers. The subunit structure of the oligomers was determined by SAXS, which is able to detect periodic structures in non-crystalline biological materials in solution (Roe, 2000; Maeshima *et al*, 2014a) and, in particular, has proven useful for determining the repetitive structures within the bulk chromatin of both mitotic chromosomes (Nishino *et al*, 2012) and intact nuclei (Joti *et al*, 2012). As in the pioneering work of Langmore and co-workers (Langmore & Paulson, 1983), scattering data are presented as plots of $\log(I \times S^2)$ versus $1/S$) [I, intensity; S, scattering vector (1/nm)]. A peak in the curve is indicative of a periodic structure in the sample with a diameter of inverse of S ($1/S$ nm) (Roe, 2000; Maeshima *et al*, 2014a). We first analyzed the structure of 601 nucleosomal arrays in 0–2.5 mM $MgCl_2$. In TE buffer without $MgCl_2$, the nucleosomal arrays sedimented at ~27S (Fig EV3), indicating that they were monomeric and in the extended 10-nm beads-on-a-string conformation (Hansen, 2002). The scattering curve of the nucleosomal arrays in 0 mM $MgCl_2$ (Fig 3A) had a broad peak between $1/S$ = 10–20 nm resulting from the distances between the nucleosomes in the extended conformation, and a minor peak at ~6 nm corresponding to the width of the nucleosome disk (face-to-face positioning) (see also Fig 3C). No peak at ~30–40 nm due to folded nucleosomal arrays (i.e. 30-nm fibers) was present under these low salt conditions, consistent with the SV-AUC data. Of note, the experimental scattering curve is very similar to the modeled scattering profile for an extended dinucleosome (Fig 3D). Addition of salt to the solution causes the nucleosomal arrays to rapidly equilibrate between 10-nm and 30-nm conformations (Hansen, 2002), resulting in a progressively increased integral distribution of sedimentation coefficients in 1 and 2.5 mM $MgCl_2$ (Fig EV3). Importantly, a small peak at ~40 nm corresponding to folded nucleosomal arrays appeared in the scattering curves in 1 and 2.5 mM $MgCl_2$ (arrow in Fig 3A), in addition to the 10- to 20-nm and 6-nm peaks that were seen for the extended 10-nm fiber. A prominent ~40-nm peak was also present in the calculated scattering profile when either solenoid or zigzag 30-nm structures made from the 12-mer nucleosomal arrays were modeled (Fig 3E and F). The experimental (Fig 3A) and modeling (Fig 3E and F) data provide important controls showing that SAXS is a valid assay for nucleosomal array folding, including being able to detect even small amounts of folded 30-nm structures when they are present.

The scattering curves obtained for the 601 oligomers assembled in 5 and 10 mM $MgCl_2$ are shown in Fig 3B. In the range of $1/S > 20$ nm, the slope of the curve was sharply downturned. This feature was observed in previous SAXS analyses of mitotic chromosomes (Nishino *et al*, 2012) and isolated nuclei (Joti *et al*, 2012),

Table 1. Physical properties of the oligomers.

S	Oligomer mass (Da)[a]	No. of arrays[b]	No. of nucleosomes[c]	Stokes R (nm)[d]	f[e]	Mb/ Oligomer[f]	% Chromosome 1[g]
5,000	1.05E+09	3.75E+02	4.50E+03	64.71	1.22E−06	0.94	0.37
25,000	1.18E+10	4.19E+03	5.03E+04	144.70	2.74E−06	10.48	4.19
75,000	6.11E+10	2.18E+04	2.61E+05	250.62	4.74E−06	54.45	21.78
150,000	1.73E+11	6.16E+04	7.39E+05	354.44	6.71E−06	154.00	61.60
300,000	4.89E+11	1.74E+05	2.09E+06	501.25	9.49E−06	435.56	174.23

[a]A minimum mass of the complexes was calculated by using a spherical shape to determine a minimum frictional coefficient for a given sedimentation coefficient. A mass can then be calculated by a rearrangement of the Svedberg equation: $S_s = \frac{M(1-\bar{\upsilon}\rho)}{NA^{6\pi\eta}\left(\frac{3\bar{\upsilon}M}{4\pi}\right)^{1/3}}$.

[b]The number of arrays was calculated by dividing the minimum mass by the theoretical mass of a saturated 12-mer array (2,805,206 Da).

[c]The estimate for the number of nucleosomes in each complex is 12 times the number of arrays.

[d]The Stokes radius is the radius of the sphere which these calculations are based on and is as follows: $r_s = \left(\frac{3\bar{\upsilon}M}{4\pi}\right)^{1/3}$.

[e]The frictional coefficient of the theoretical sphere is as follows: $f = 6\pi\eta\left(\frac{3\bar{\upsilon}M}{4\pi}\right)^{1/3}$.

[f]As each 12-mer array contains 2.5 kb of DNA, the number of arrays in a complex was used to determine the number of bp.

[g]The percentage of chromosome one was based on the Mb of DNA per oligomer divided by 250 Mb.

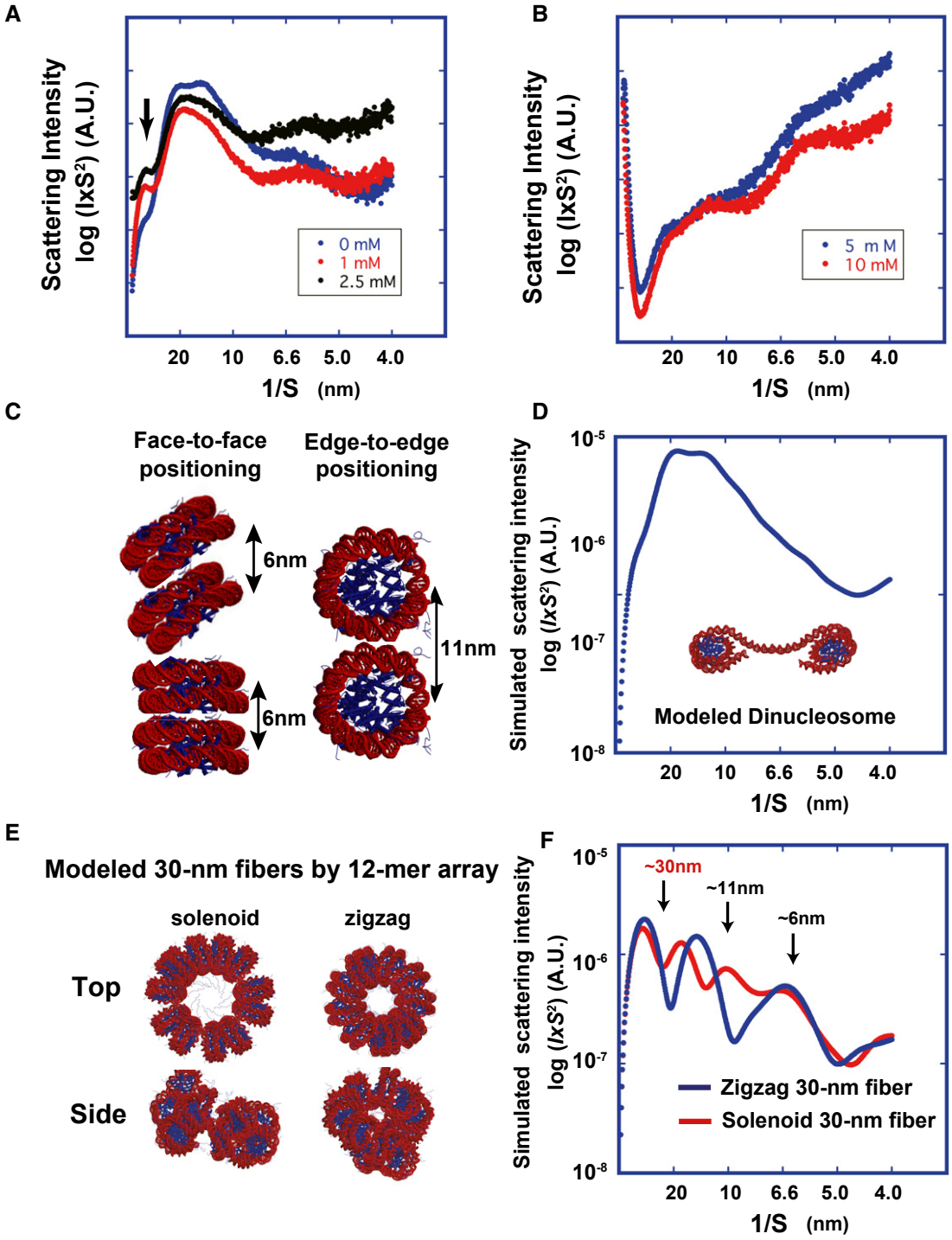

Figure 3. SAXS profiles of nucleosomal array oligomers and reconstructed *in silico* models.

A, B SAXS profiles of the nucleosomal arrays in 0 (TE), 1, 2.5 mM $MgCl_2$ (A), and 5, 10 mM $MgCl_2$ (B) are shown as plots of $\log(I \times S^2)$ versus $1/S$ [I, intensity; S, scattering vector (1/nm)].

C Two types of nucleosome positioning: face-to-face, at ~6-nm spacing, and edge-to-edge, at ~11-nm spacing. The image was made based on the structural information published in Luger *et al* (1997).

D The modeled scattering profile of an extended dinucleosome structure based on its atomic coordinate (for details, see Materials and Methods). Note that the modeled profile is similar to that of the nucleosomal arrays in 0 mM $MgCl_2$ (A).

E Two structural models of 12-mer 30-nm fibers: solenoid (left) and zigzag (right) as a top and side view. The models were constructed using MolScript (Kraulis, 1991).

F The scattering profiles of the solenoid (red line) and zigzag (blue line) 30-nm fibers were made from their atomic coordinates computationally. Note that the 30- to 40-nm peak is prominent in both fiber models.

and results from the very large size of the oligomers. No ~40-nm peak was observed in the oligomer samples, indicating that the nucleosomal array subunits were not in a folded 30-nm conformation. The broad peaks at $1/S$ = 10–20 nm and 6 nm seen for the extended arrays (Fig 3A) were still present in the oligomeric samples, although between $1/S$ = 4–30 nm the slope of the curve was sharply positive (Fig 3B). For proteins, the upward slope is characteristic of a denatured polypeptide chain (Doniach, 2001), implying that the nucleosomal arrays remain somewhat mobile within the oligomers. Collectively, the SAXS analyses of monomeric and oligomeric nucleosomal arrays indicate that the oligomers consist of packaged 10-nm fibers.

We next asked whether the packaged linker DNA within the oligomers could be completely digested by MNase and if so, whether the oligomers remained intact after digestion. Nucleosomal arrays were incubated in digestion buffer containing either 0.5 or 5 mM $MgCl_2$. The arrays were ~100% monomeric in 0.5 mM $MgCl_2$ and ~85% oligomeric in 5 mM $MgCl_2$ as judged by the differential centrifugation assay (Fig 4A). For the oligomers in 5 mM $MgCl_2$, the presence of only mononucleosomal DNA in the deproteinized MNase digest indicated that the linker DNA was completely accessible and digested to completion under the conditions used (Fig 4B). When the oligomers in 5 mM $MgCl_2$ were digested to completion with MNase and examined by FM, we still observed oligomeric particles, but both the size (Fig 4C) and the number (Fig 4A) of the oligomers were reduced compared to the undigested control. Thus, both attractive nucleosome–nucleosome interactions (Liu *et al*, 2011) and linker DNA contribute to oligomer stability.

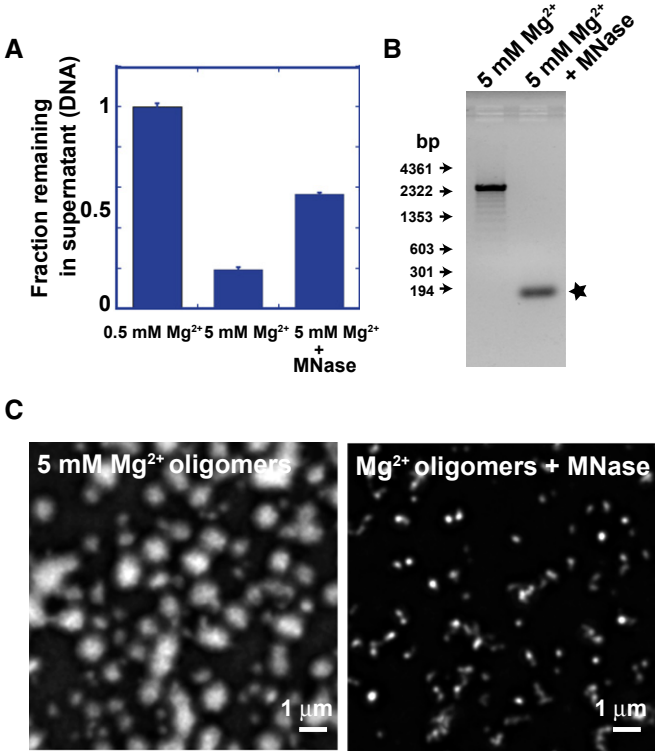

Figure 4. Effect of MNase digestion on oligomer structure.

A 601 nucleosomal arrays were incubated in 0.5, 5 mM $MgCl_2$, 5 mM $MgCl_2$ + MNase and analyzed by the differential centrifugation assay to determine the fraction oligomeric. The amounts of DNA in the supernatant fraction were measured. Note that for the MNase-digested oligomers, the supernatant fraction also includes the digested free linker DNA. Each value is the mean of three measurements, and the error bars represent the standard deviation.

B Verification of complete MNase digestion. DNA was purified from the nucleosomal arrays incubated in 5 mM $MgCl_2$ or 5 mM $MgCl_2$ + MNase and then electrophoresed on agarose gel. The position of mononucleosome is marked with a star symbol.

C Nucleosomal array oligomers without (left) or with MNase treatment (right) were stained with DAPI and examined using FM. Shown are representative images obtained. Note that the sizes of MNase-treated oligomers are much smaller than those of the control oligomers (left and Fig 1A).

Linker histones modulate oligomer structure, assembly, and subunit packaging

Linker histones are the most abundant chromatin-associated proteins in most eukaryotic cells (Woodcock *et al*, 2006) and promote chromatin condensation *in vitro* (Hansen, 2002) and *in vivo* (Fan *et al*, 2005; Hashimoto *et al*, 2010). We therefore determined how linker histones affected nucleosomal array oligomerization. When characterized by the differential centrifugation assay, the plot for the H1-bound nucleosomal arrays was shifted to the left relative to that obtained for the nucleosomal arrays alone, although the shapes of the curves otherwise were very similar (Fig EV1A). While this indicates that linker histones in some way influence oligomerization, to more quantitatively address this question the H1-bound nucleosomal arrays were characterized by microscopy, SV-AUC, and SAXS as a function of salt.

Typical FM images obtained in 4 and 5 mM $MgCl_2$ for the 601 H1-oligomers are shown in Fig 5A. The H1-oligomers visualized in 4 and 5 mM $MgCl_2$ (~75% and 90% oligomerized, respectively) were globular and ~100–300 nm in size. Control FM images in 0, 1, and 3 mM $MgCl_2$ are shown in Fig 5B. Very small particles were faintly visible in 1 and 3 mM $MgCl_2$ but not at the lower salt concentration. In 4 mM $MgCl_2$ the predominant oligomers observed by TEM were globular and had diameters of ~200–300 nm (Fig 5C, left), consistent with the diameters seen in the FM images under the same conditions (Fig 5A). As with the nucleosomal array oligomers (Fig 1C, right panels), at higher magnification one could see individual closely packed nucleosomes, but no regular repetitive folded structures such as the 30-nm fiber (Fig 5C, right panel).

The s_{sm} of the H1-oligomers as a function of $MgCl_2$ is shown in Fig 6A. The s_{sm} in 3 mM $MgCl_2$ was ~650S, which increased to ~13,000S in 4 mM $MgCl_2$. While these sedimentation coefficients are very large, the s_{sm} of the H1-oligomers was smaller than the s_{sm} of the nucleosomal array oligomers under equivalent extents of self-association (Fig EV4A), consistent with the FM analysis (compare Figs 1A and 5A). Above 5 mM $MgCl_2$, the oligomers pelleted immediately and the s_{sm} was too large to measure, even with the interference optical system (Fig 6A). Analysis by the time-derivative method yielded the distribution of H1-oligomer sedimentation coefficients present at each salt concentration. In 3 mM $MgCl_2$, the sedimentation coefficient distribution ranged from ~200 to 1,400S, with a peak in the plot at ~600S (Fig 6B and C). In 3.5 mM $MgCl_2$, the distribution of observed sedimentation coefficients was shifted to ~600–3,000S, and the peak in the g(s) plot increased to ~1,100S

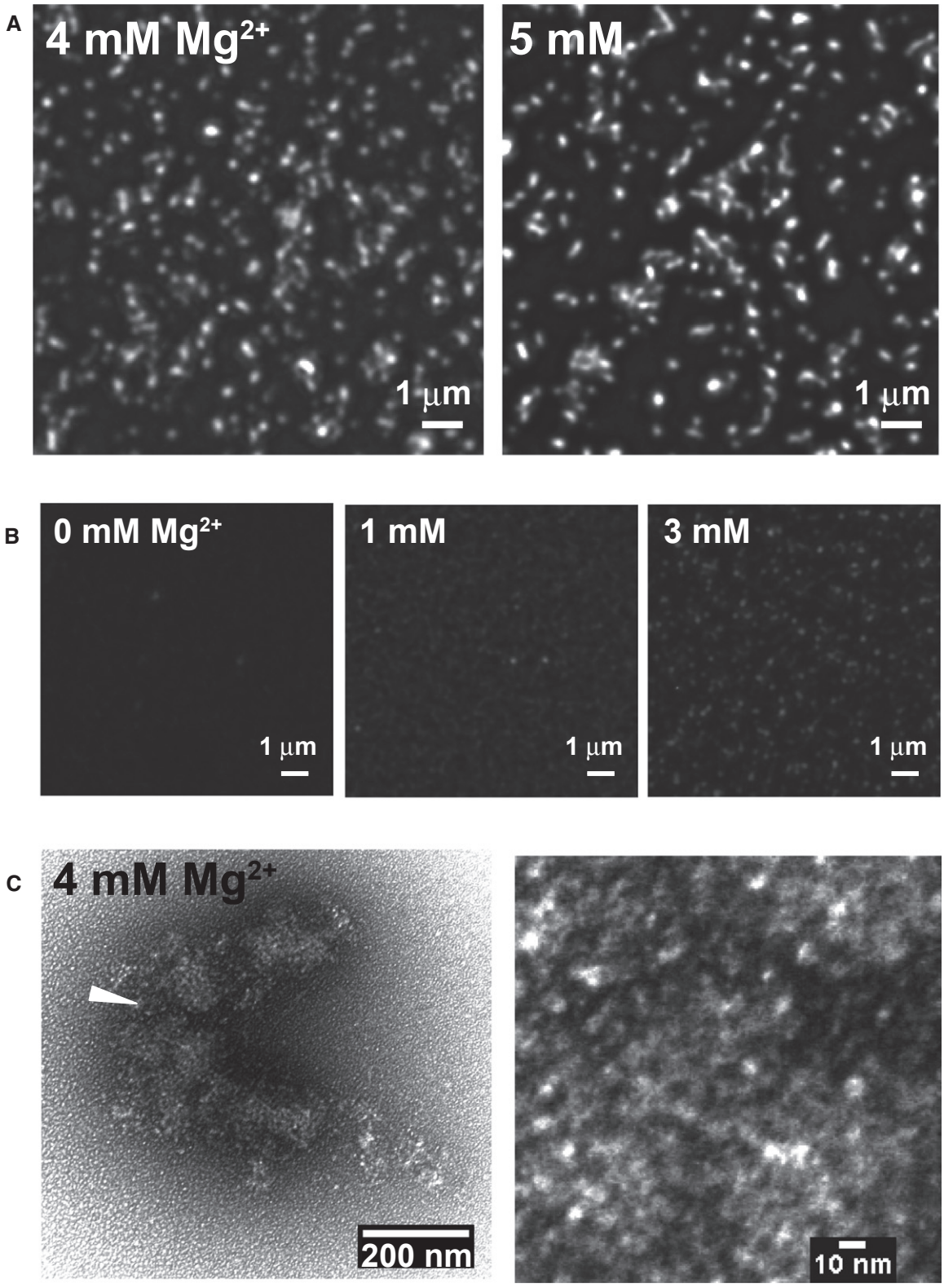

Figure 5. H1-oligomers are globular.

A Oligomers assembled from H1-nucleosomal arrays were stained with DAPI and examined using FM. Shown are representative images obtained in 4 and 5 mM $MgCl_2$.

B Control FM images obtained in 0, 1, and 3 mM $MgCl_2$.

C H1-nucleosomal array oligomers were negatively stained and visualized by TEM. Shown in the left panel is a representative image obtained in 4 mM $MgCl_2$. Shown in the right panel is an image of the interior of the oligomer (white arrow, left panel) after cropping and rescaling.

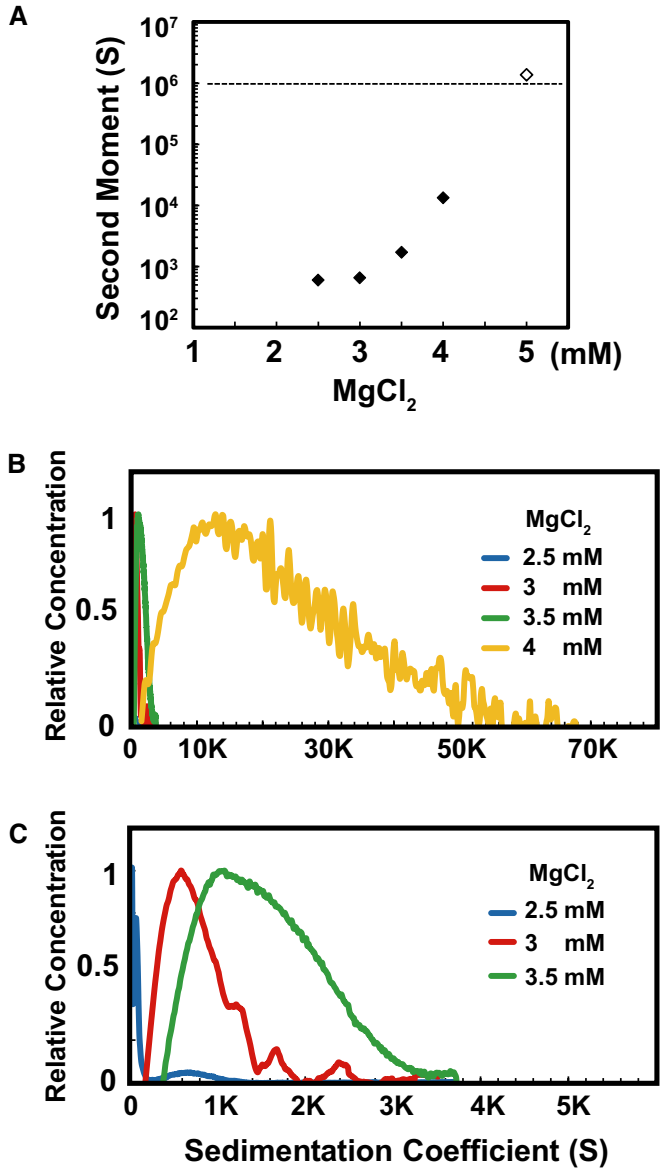

Figure 6. Sedimentation analysis of salt-dependent H1-oligomer assembly.

A Representative experiment showing the second moment sedimentation coefficients of the H1-oligomers as a function of $MgCl_2$. The dashed line indicates the upper limit of measurable sedimentation coefficients (~10^6 S). The white symbol is intended to show that the sedimentation coefficient of the H1-oligomers in 5 mM $MgCl_2$ is beyond the detectable limit.

B Analysis of the same raw data as in (A) by the time-derivative method to yield the sedimentation coefficient distribution, g(s*).

C The g(s*) profiles in 2.5, 3, and 3.5 mM from (B) are re-plotted on a smaller scale.

(Fig 6C). In 4 mM $MgCl_2$, the range of H1-oligomer sedimentation coefficient increased significantly, extending from ~2,000 to 50,000S with a peak in the g(s) plot at ~12,000S (Fig 6B). To directly determine the effect of H1 on oligomer size, the oligomer sedimentation coefficient distributions determined in 4 mM $MgCl_2$ in the absence and presence of H1 were converted to Mb DNA/oligomer (as in Table 1). In both cases, the DNA content of the H1-oligomers ranged from < 1- to ~30 Mb/oligomer. However, the average for the H1-oligomers was 4-Mb DNA/oligomer compared to 12-Mb DNA/oligomer for the nucleosomal array oligomers under these conditions (Fig EV4B).

Given that H1 stabilizes folded 30-nm structures *in vitro* (Hansen, 2002; Robinson & Rhodes, 2006; Li & Zhu, 2015), we wanted to determine whether the subunit structure of the H1-oligomers was the 30-nm fiber. As a control, we first compared the results obtained by SV-AUC and SAXS for H1-bound nucleosomal arrays in 0–2.5 mM $MgCl_2$. In 0 mM $MgCl_2$, the H1-arrays sedimented at ~32S (Fig EV5), indicating that they were monomeric and extended (Carruthers *et al*, 1998). The scattering curve of the H1-arrays in 0 mM $MgCl_2$ resembled that of parent nucleosomal arrays under the same conditions, with a broad peak at 10–20 nm, a minor peak at ~6 nm, but no peak at ~30–40 nm corresponding to folded fibers (Fig 7A). This indicates that the H1-bound arrays in the absence of salt had an extended structure with 10- to 20-nm internucleosomal distances in solution. In 1 mM $MgCl_2$, the H1-arrays began to form folded structures, as indicated by the increase in the maximum sedimentation coefficient to 45S (Fig EV5). Under these conditions, a significant peak at 30–40 nm appeared in the SAXS profile (arrow in Fig 7A), consistent with the similar peak seen for the modeled 30-nm fibers (Fig 3E and F). SV-AUC analysis of the H1-array samples in 2.5 mM $MgCl_2$ indicated two major populations of fibers; one sedimented at ~32–55S, while the other sedimented from ~90 to 130S. The former corresponds to a distribution of folded monomers, while the latter is indicative of small oligomers that do not pellet at 662 *g*. Importantly, the SAXS profile in 2.5 mM $MgCl_2$ was dominated by a major peak at 30–40 nm. A comparison of the SAXS data for monomeric nucleosomal arrays (Fig 3A) and H1-bound arrays (Fig 7A) demonstrates that H1 stabilizes folded 30-nm fibers, as has been observed by SV-AUC (Fig EV5) and other techniques (Robinson & Rhodes, 2006; Li & Zhu, 2015).

SAXS analyses of the H1-oligomers assembled in 5 and 10 mM $MgCl_2$ are shown in Fig 7B. In the range of $1/S > 20$ nm, the slopes of the curves were sharply downturned due to the large size of the oligomers. The ~30- to 40-nm peak seen in the 1 and 2.5 mM $MgCl_2$ control samples was absent in the H1-oligomers. Between $1/S = 4$–10 nm, the slopes of the scattering curves were flat and prominent peaks at 6 and 11 nm were apparent (Fig 7B). The 6- and 11-nm peaks have been proposed to come from edge-to-edge and face-to-face positioning of nucleosomes, respectively (Langmore & Paulson, 1983) (see Fig 3C). Several important conclusions can be drawn from these data. First, the 12-mer nucleosomes within the H1-oligomers were not folded into regular 30-nm fibers. Second, H1 abolished the upward slope between $1/S = 4$–10 nm seen in the plots of the nucleosomal array oligomers (Fig 3B), suggesting tighter subunit packing. Lastly, H1 sharpened the diffuse 6- and 11-nm peaks present in the control H1 samples (Fig 7A) and the nucleosomal array oligomers (Fig 3B). The scattering curves for isolated native chicken chromatin fragments (which contain heterogeneous linker DNA lengths and near stoichiometric levels of H1) were similar to those obtained for the 601 H1-arrays, but with lower concentration of $MgCl_2$ (Fig 7C), indicating that SAXS results were not dependent on the regular positioning of the 601 arrays. We next modeled the SAXS curve for *in silico* oligomers composed of 100 randomly and tightly packed 12-mer nucleosomal arrays in the 30-nm conformation (Fig 7E and F). The nucleosome concentration

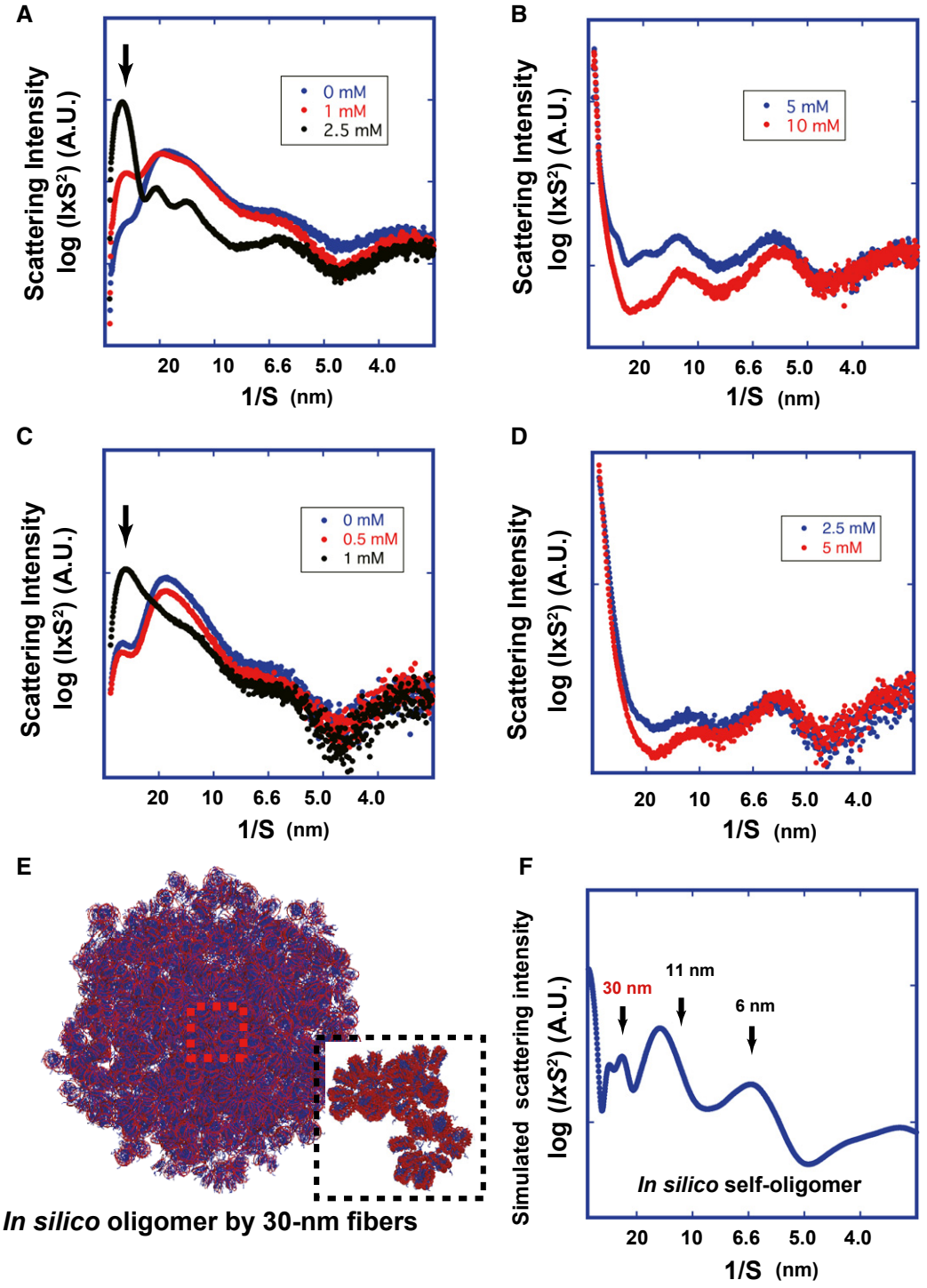

Figure 7. SAXS profiles of the H1-oligomers, native chicken chromatin, and reconstructed *in silico* oligomer models.

A, B SAXS profiles of the H1-nucleosomal arrays in 0 (TE), 1, 2.5 mM $MgCl_2$ (A), and 5, 10 mM $MgCl_2$ (B) are shown as plots of $\log(I \times S^2)$ versus $1/S$ [I, intensity; S, scattering vector (1/nm)].

C, D SAXS profiles of the native chicken chromatin in 0 (TE), 0.5, 1 mM $MgCl_2$ (C), and 2.5, 5 mM $MgCl_2$ (D) are shown as plots of $\log(I \times S^2)$ versus $1/S$ [I, intensity; S, scattering vector (1/nm)].

E The "*in silico* oligomer" models were constructed in environments containing 100, 50, and 25 randomly and tightly packed 12-mer 30-nm fiber models (Fig 3E). The nucleosome concentration was 0.5 mM. The 100-fiber model was drawn using MolScript (Kraulis, 1991). The broken-lined squares show magnified regions.

F The modeled scattering profiles, yielding average among-model values, have prominent peaks at ~30–40, 11, and 6 nm. This shows that the *in silico* oligomers retain characteristics of 30-nm fibers. Note that the modeled scattering profile is very distinct from the SAXS profiles in (B) and (D), Fig 3B, and Fig 8B (center and right).

of the *in silico* oligomers was about ~0.5 mM, comparable to that of mitotic chromosomes (Hihara *et al*, 2012). The scattering profile of the *in silico* oligomers closely resembled the experimental scattering profile for the H1-oligomers, except for the presence of peaks at ~30–40 nm in the modeled curve (arrow in Fig 7F). The modeling results further support the conclusion that the subunit structure of the H1-oligomers is not the folded 30-nm fiber.

Low salt disassembles higher-order chromatin structures in nuclei *in situ*

Our *in vitro* studies suggest that the oligomers formed by nucleosomal arrays in the absence and presence of histone H1 are good *in vitro* models for interphase chromosome structure in nuclei. Given that the oligomers are stable in 5 mM $MgCl_2$, but not in < 1 mM $MgCl_2$ (Fig EV1), we predicted that chromatin structure and organization *in situ* would appear normal in 5 mM $MgCl_2$, but would be disrupted by exposure to EDTA, which reduces the $MgCl_2$ concentration to essentially zero. To test our hypothesis, the effects of $MgCl_2$ on the higher-order chromatin structures present *in situ* in isolated HeLa nuclei were determined using FM and SAXS. To visualize nuclear structure, isolated nuclei were exposed to DAPI and analyzed by FM. In 1 and 5 mM $MgCl_2$, all of the nuclei examined showed bright regions resulting from areas of intense DAPI staining (heterochromatin-rich) interspersed with dark regions that were less concentrated with DAPI (euchromatin) (Fig 8A, center and right panels). The DAPI-intense regions were especially prominent near the nuclear periphery and around nucleoli. These images show that canonical interphase chromatin organization is retained in 1 and 5 mM $MgCl_2$. In distinct contrast, uniform DAPI staining was observed in nuclei exposed to EDTA (Fig 8A, left panel), demonstrating that higher-order chromatin organization *in situ* was disrupted in the absence of cations. Quantitation of the nuclear sizes indicated that the nuclei in EDTA on the average were twice as large as those in 1 and 5 mM $MgCl_2$ (Fig 8A), indicative of extensive chromatin decondensation. Independently, SAXS analysis of HeLa nuclei was used to examine bulk interphase chromatin as a function of salt. The scattering profiles in 1 and 5 mM $MgCl_2$ (Fig 8B, center and right panels) closely resembled those observed previously for intact nuclei (Joti *et al*, 2012), and the H1-oligomers (Fig 7B), with a prominent downturned slope in the range of $1/S > 15$ nm and peaks at 6 and 11 nm. This indicates that the *in vitro* assembled oligomers and HeLa nuclear chromatin are packaged similarly in the presence of $MgCl_2$. When the isolated HeLa nuclei were incubated in EDTA buffer, the scattering profile (Fig 8B, left panel) changed to one that more closely resembled those of the nucleosomal array and H1-nucleosomal array monomers (Figs 3A and D, and 7A). It should be noted that 30- to 40-nm peak seen in HeLa nuclei in EDTA buffer most likely results from the spatial constraint of the extensively decondensed chromatin present under these conditions, not from the presence of folded 30-nm chromatin fibers (e.g. see Fig 4 in Eltsov *et al*, 2008). The FM and SAXS results together demonstrate that higher-order chromatin structure in isolated nuclei *in situ* is disassembled in the absence of cations, conditions that also dissociate oligomeric nucleosomal arrays *in vitro*. These results further indicate that HeLa nuclear chromatin *in situ* is stabilized by lower $MgCl_2$ concentration (~1 mM) than the nucleosomal array oligomers and H1-oligomers, probably because the nuclear chromatin is at much higher concentration and complexed with more proteins than the model systems used in the *in vitro* experiments. The differential centrifugation assay of isolated HeLa chromatin is a good agreement with this finding, that is, the $MgCl_2$ concentration at which 50% of the sample pellets (Mg^{50}) for the oligomerization of the HeLa chromatin is ~1 mM $MgCl_2$, compared to ~2.5 mM $MgCl_2$ for H1-nucleosomal arrays and ~4 mM $MgCl_2$ for nucleosomal arrays (Appendix Fig S3 and Fig EV1).

Discussion

The oligomers characterized in our studies recapitulate key aspects of interphase chromosome structure and organization. Interphase chromosomes occupy discrete territories within the nucleus, and the territories appear globular when visualized by fluorescence *in situ* hybridization (Cremer & Cremer, 2010). Studies using chromosome conformation capture technology and its variants suggest that the long linear chromosomal chain of nucleosomes (Valouev *et al*, 2011) is assembled into arrays of higher-order globular chromatin domains, often called topologically associating domains. Globular chromosomal domains also have been observed by fluorescence microscopy (Albiez *et al*, 2006). A typical chromatin domain contains ~0.1–10 Mb of DNA (Dekker *et al*, 2013; Rao *et al*, 2014; Eagen *et al*, 2015). In the case of *in vitro* oligomerization, the early stages of nucleosomal array self-association produce globular particles containing ~1- to 10-Mb DNA/oligomer (Fig 2, Table 1). At their maximum, the globular oligomers are the size of chromosomes. When H1 is bound to nucleosomal arrays *in vitro*, the early stages of self-association produce globular oligomers consisting of ~0.5- to 1.0-Mb DNA/oligomer, quite similar to the average size observed for the chromatin domains in nuclei (Dekker *et al*, 2013; Rao *et al*, 2014; Eagen *et al*, 2015). These observations indicate that the globular oligomers characterized in our studies span the size range of the chromatin domains present in nuclei, and suggest that the oligomers are good *in vitro* model systems for studying interphase chromosome structure and organization.

The single nucleosome fiber that makes up an interphase chromosome behaves as a flexible random coil polymer chain, for example (Barbieri *et al*, 2014). Thus, widely separated stretches of chromosomal nucleosomes will be able to interact over Mb distances, and the self-association of 12-mer nucleosomal arrays should be an *in vitro* reflection of the self-interactions of a condensed chromosomal fiber. The biological relevance of nucleosome oligomerization was addressed experimentally by examining the effect of $MgCl_2$ concentration on the structure of isolated human nuclei. In our hypothesis, the conditions that disassemble the oligomers *in vitro* should disrupt long-range chromosomal fiber interactions and perturb higher-order chromatin structure in the nucleus. Our FM and SAXS analyses of isolated nuclei demonstrate that the heterochromatin and euchromatin compartments present in ~1 mM $MgCl_2$ *in situ* were abolished by exposure to EDTA, concomitant with extensive chromatin decondensation (Fig 8). In recent related studies, chromatin condensation within permeabilized cell nuclei increased dramatically as the divalent cation and polyamine concentration were increased from 0 mM into the physiological range (Visvanathan *et al*, 2013), and hypotonic treatment (low salt) in living mammalian cells caused extensive chromatin

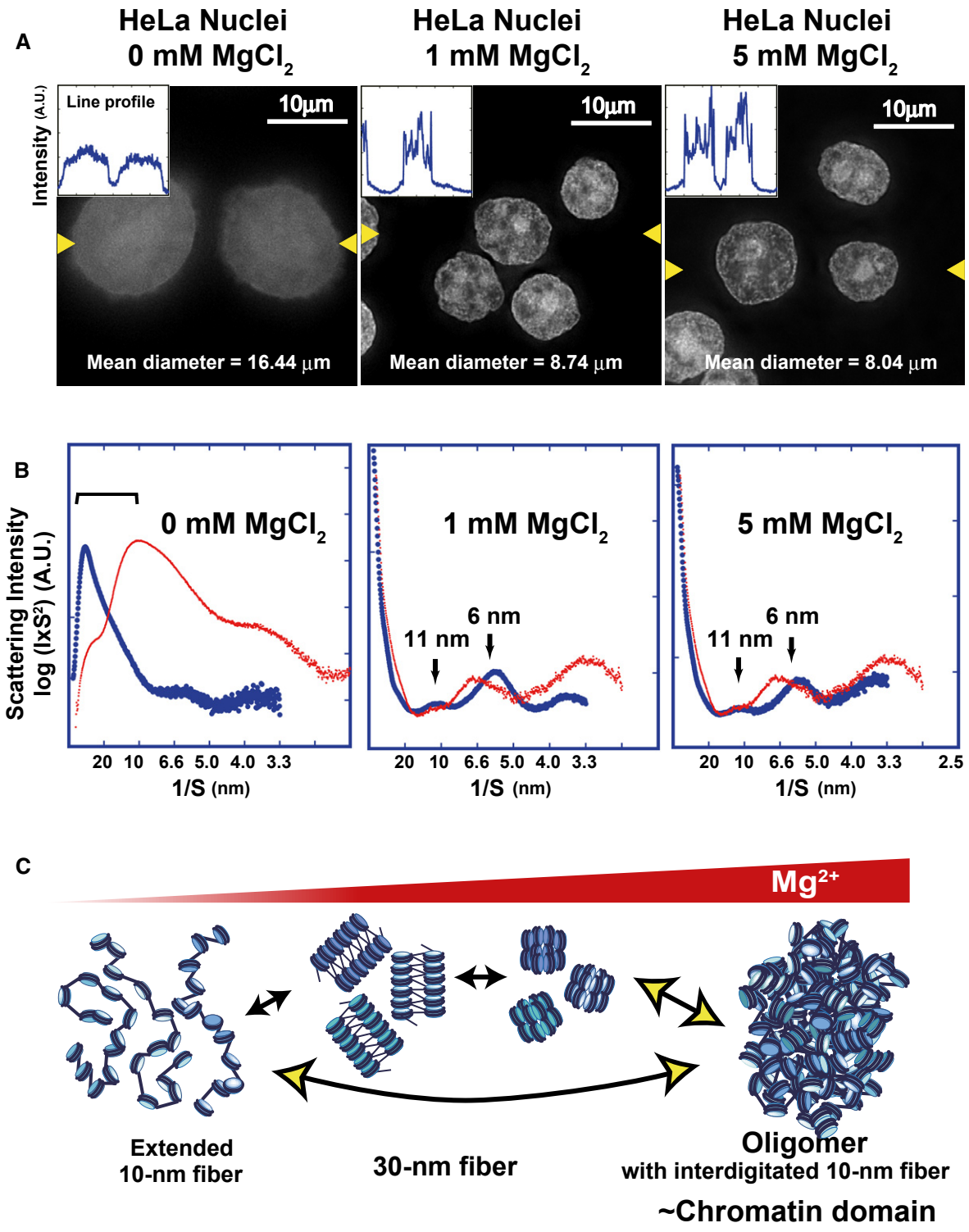

Figure 8. Effect of $MgCl_2$ concentration on the chromatin structure of isolated HeLa nuclei.

A FM images of chromatin structure in the nuclei with 0 (left), 1 (center), and 5 mM $MgCl_2$ (right). Insets show the intensity line profiles between the two marked arrow heads in the images.

B SAXS profiles of the isolated HeLa nuclei. SAXS profiles of the nuclei in 0 (left), 1 (center), and 5 mM $MgCl_2$ (right) are shown in blue. For comparison, the scattering curves of H1-arrays from Fig 7A and B were overlaid as red lines (left, 0 mM; center and right, 10 mM $MgCl_2$).

C Model scheme. The 12-mer nucleosomal array is a well-defined model chromatin system. In 1–2 mM Mg^{2+}, the nucleosomal array folds into a folded 30-nm chromatin fiber structure. With further increases in Mg^{2+}, the nucleosome arrays assemble into supramolecular oligomers. The large oligomers are not assemblies of the 30-nm chromatin fibers, but are proposed to be interdigitated and melted structures of 10-nm nucleosomal arrays.

decondensation (Albiez *et al*, 2006). Collectively, the *in situ* results indicate that very low salt concentrations that destabilize nucleosome oligomers *in vitro* also destabilize the chromatin domains and higher-order chromatin structures in isolated nuclei. This in turn suggests that core and linker histone-mediated long-range nucleosome–nucleosome interactions contribute significantly to interphase chromosome structure and organization. Of note, histone-mediated long-range nucleosome–nucleosome interactions also appear to be applicable to mitotic chromosome structure. Isolated mitotic chromosomes behave like interphase chromatin in the presence and absence of salt. Without $MgCl_2$, the chromosomes are highly swollen and the chromosomal fibers are stretched into 10-nm-like fibers (Earnshaw & Laemmli, 1983; Eltsov *et al*, 2008; Takata *et al*, 2013), whereas in the presence of $MgCl_2$, the chromosomes are highly condensed (Earnshaw & Laemmli, 1983; Eltsov *et al*, 2008; Takata *et al*, 2013). Mg^{2+}-dependent mitotic chromosome decondensation and condensation are highly reversible (Hudson *et al*, 2003).

The widely held paradigm for chromosomal DNA packaging *in vivo* maintains that helical 30-nm chromatin structures are requisite folding intermediates in the establishment of higher-order chromosomal domains, that is, the nucleosome chain must first fold into 30-nm fibers before assembling into successively more condensed chromatin structures (for reviews, e.g. Hansen, 2002; Robinson & Rhodes, 2006; Grigoryev & Woodcock, 2012; Maeshima *et al*, 2014b; Li & Zhu, 2015). This view is based in large part on the fact that 10-nm fibers initially fold into 30-nm fibers when salt is titrated into solution *in vitro*. However, there is very little direct evidence for the existence of bulk 30-nm fibers in chromosomes. Although a ~30- to 40-nm peak was observed in SAXS studies of living cells, isolated nuclei, and mitotic chromosomes (Langmore & Paulson, 1983; Joti *et al*, 2012; Nishino *et al*, 2012), if the nuclei and mitotic chromosomes were first stripped of contaminating ribosomes, the ~30- to 40-nm peak was absent (Joti *et al*, 2012; Nishino *et al*, 2012). Consistent with these results, cryo-EM studies of interphase chromatin and mitotic chromosome (Bouchet-Marquis *et al*, 2006; Eltsov *et al*, 2008; Gan *et al*, 2013) and electron spectroscopic imaging studies of mouse nuclei (Fussner *et al*, 2012) visualized packaged 10-nm fibers, but no folded 30-nm fibers, even in the heterochromatin regions. Recent studies using super-resolution imaging also observed heterogeneous groups of nucleosomes (Ricci *et al*, 2015). Collectively, these studies argue for a new chromosome assembly paradigm that does not require folding into 30-nm fibers. Our SAXS analysis of the packaging of nucleosomal array oligomers provides biochemical evidence in support of an alternative model. In our control SAXS experiments, folding of monomeric arrays into 30-nm structures in 2.5 mM $MgCl_2$ was indicated by the appearance of a peak in the scattering profile at ~30–40 nm (Figs 3A and 7A). However, this peak was noticeably absent in the SAXS profiles of both the H1-bound and H1-free oligomers, indicating that the subunit structure of the oligomers is not the 30-nm fiber. Instead, the lack of observed repetitive structures above 20 nm indicates that the subunits adopt extended 10-nm structures. We thus conclude that when studied *in vitro* nucleosomal arrays and H1-chromatin only form 30-nm fibers under very specific ionic conditions. In addition, given that the peaks at 6 and 11 nm arise from face-to-face and edge-to-edge nucleosome–nucleosome interactions, respectively (Fig 3C) (Langmore & Paulson, 1983), and the fact that linker DNA contributes to oligomer stability (Fig 4), we propose that the individual 10-nm nucleosomal array subunits interdigitate to form a polymer melt-like structure when packaged into the oligomers. Our studies ultimately provide a rigorous biochemical basis for how long-range chromatin condensation can occur without first forming 30-nm fibers.

Oligomerization absolutely requires the core histone tail domains of the nucleosome. Tailless nucleosomal arrays do not self-associate (Schwarz *et al*, 1996; Dorigo *et al*, 2003; Gordon *et al*, 2005), even in the presence of linker histones (Carruthers & Hansen, 2000). When the H2A, H2B, H3, and H4 tail domains are deleted individually, in each case the Mg^{50} is shifted toward higher $MgCl_2$ concentrations (Dorigo *et al*, 2003; Gordon *et al*, 2005). Removal of the H4 tail has the largest effect on the Mg^{50} (Dorigo *et al*, 2003; Gordon *et al*, 2005), suggesting that it is a particularly important determinant. The need for more $MgCl_2$ when the tails are deleted implies that they function through an electrostatic-based mechanism. We speculate that the tails at least in part bind to linker DNA and screen negative charge, promoting interdigitated nucleosome–nucleosome interactions and oligomer assembly. In support of this hypothesis, the H4 and H3 tails can be cross-linked in *trans* to the DNA of other arrays within the packaged oligomers (Zheng *et al*, 2005; Kan *et al*, 2009). Moreover, linker DNA contributes significantly to oligomer stability (Fig 4), as would be expected if it was the binding site for the tails. The H4 tail domain mediates 30-nm fiber folding by binding the acidic patch present on the surface of neighboring nucleosomes (Kalashnikova *et al*, 2013). However, oligomerization and 30-nm folding are mediated by distinct molecular mechanisms, and in particular, oligomerization does not require H2A/H2B (Schwarz *et al*, 1996). The involvement of the H4 tail in both folding and oligomerization, acting through different mechanisms, provides a potential explanation for why the subunits of the oligomers adopt the 10-nm fiber structure. That is, under conditions where the H4 tails mediate oligomerization, they cannot simultaneously interact with the acidic patch of neighboring nucleosomes to promote 30-nm folding. Certain tail post-translational modifications affect the Mg^{50}, including H4 acetylation (Shogren-Knaak *et al*, 2006; Szerlong *et al*, 2010), H4 sumoylation (Dhall *et al*, 2014), and both H2A and H2B ubuiquitination (Jason *et al*, 2001; Fierz *et al*, 2011). Nucleosome-depleted regions such as those found near promoters and enhancers, and the core histone variant H2A.Z (Fan *et al*, 2002), move the Mg^{50} toward higher $MgCl_2$ concentrations relative to nucleosomal arrays alone. The macroH2A variant (Muthurajan *et al*, 2011) and chromatin architectural proteins such as MeCP2 (Nikitina *et al*, 2007) and Sir3p (McBryant *et al*, 2008) all lower the $MgCl_2$ concentration at which oligomerization occurs. The large number of physiologically relevant determinants of oligomerization suggests that the equilibrium between local and global nucleosome–nucleosome interactions in any given region of a chromosomal fiber is a tightly regulated point of regulatory control.

Materials and Methods

Reconstitutions

Nucleosomal arrays were reconstituted from 12 × 207 bp 601 or 5S sequence DNA and purified chicken erythrocyte histone octamers

using salt dialysis as described (Rogge *et al*, 2013). The DNA concentration was 0.5 mg/ml, and molar ratio of histone octamers to DNA repeats was 1.0–1.1. The extent of template saturation achieved after reconstitution was determined by sedimentation velocity in low salt (Hansen & Lohr, 1993). The nucleosomal arrays used in our studies sedimented between 26–29S in TE buffer (Figs EV2 and EV3), indicating that about half of the samples contained 11 nucleosomes per template and the other half contained 12 nucleosomes per template (Hansen & Lohr, 1993). H1-nucleosomal arrays were assembled by mixing purified chicken H1.0 (Talbert *et al*, 2012) and reconstituted nucleosomal arrays at one H1 per DNA repeat in 50 mM NaCl, followed by dialysis against TE buffer overnight and sedimentation velocity in low salt to determine the extent of H1 binding (Lu *et al*, 2009).

Fluorescence light microscopy of nucleosomal arrays and isolated nuclei

Two micrograms of nucleosomal array and H1-nucleosomal array samples was incubated with the desired concentration of $MgCl_2$ for 15 min on ice and spun onto poly-L-lysine-coated coverslips by centrifugation at 2,380 *g* for 15 min. The arrays were gently fixed with 2% formaldehyde (Wako, Japan) in the same buffer. After DNA staining with 4′,6-diamidino-2-phenylindole (DAPI), the coverslips were sealed with a nail polish. Optical sectioning images with 200 nm thickness were recorded with DeltaVision microscope (Applied Precision) and deconvolved to remove out of focus information. Projected images with five sections were shown.

For nuclei imaging, HeLa nuclei isolation was performed as described previously (Takata *et al*, 2013). Isolated nuclei were suspended in H10Mg5 buffer (10 mM HEPES–KOH [pH 7.4] and 5 mM $MgCl_2$) and attached to poly-L-lysine-coated coverslips by centrifugation at 2,380 *g* for 15 min. The nuclei on the coverslips were gently placed in the following three buffers: H10Mg5, H10Mg1 [10 mM HEPES–KOH (pH 7.4) and 1 mM $MgCl_2$], H10E [10 mM HEPES–KOH (pH 7.4) and 1 mM EDTA (pH 8.0)] buffers and then fixed with 2% formaldehyde in the same three buffers. After DNA staining with DAPI, the coverslips were sealed with a nail polish. Sectioning images were recorded and demonstrated as described above.

Transmission electron microscopy

Nucleosomal array or H1-nucleosomal array samples were incubated with the desired concentration of 30X $MgCl_2$ for 30 min at room temperature and fixed with 0.1% glutaraldehyde overnight on ice. The DNA concentration was 0.215 mg/ml. Samples (10 μl drops) were deposited on freshly glow-discharged formvar- and carbon-coated copper grids for 2 min, either with no dilution or at 1:20 and 1:40 dilutions. Excess sample was removed from the grids by blotting. The grids were successively stained for 2 min with 2% uranyl acetate, sample buffer, and 1.5% phosphotungstic acid, with blotting in between each. The grids were then examined and photographed using either a JEOL JEM-2000 EX II transmission electron microscope operated at 100 kV and captured on film, or a JEOL JEM-1400 transmission electron microscope equipped with an Orius model 832.J76VV0 (Gatan, Inc.) digital camera and operated at 100 kV. Images were collected at microscope magnifications from 30,000 to 300,000. Negatives were scanned at 1,200 dpi using an Epson Perfection V700 photo scanner and Adobe Photoshop. Images of the grids were processed using ImageJ for figures. Magnified images of the oligomer interiors were obtained by cropping and rescaling the initial images in order to make fine details more apparent.

Analytical ultracentrifugation

Sedimentation velocity analyses were carried out in a Beckman XL-A or XL-I analytical ultracentrifuge. Experiments measuring the salt-dependent folding of nucleosomal arrays and H1-nucleosomal arrays were performed using the absorbance optical system as described (Lu *et al*, 2009). Absorbance sedimentation velocity data were analyzed by the method of Demeler and van Holde (2004) to yield the diffusion-corrected integral distribution of sedimentation coefficients. Experiments characterizing nucleosomal array and H1-nucleosomal array oligomers were performed using the interference optical system as described (Rogge & Hansen, 2015). The laser delay and duration for a sharp fringe pattern were determined using a sapphire window cell containing only buffer. The counterbalance was then used for radial calibration of the detector. For each interference sedimentation velocity run, a single nucleosomal array and H1-arrays sample was prepared to a final concentration of 0.215 mg/ml DNA and the desired 30X $MgCl_2$ concentration, loaded into a cell assembled with sapphire windows, and placed in an An60-Ti rotor. The temperature of the run was 20°C. The speed of the runs initially was 662 *g*. After the collection of 20–60 interference scans at this speed, the oligomeric fraction of the sample had pelleted. The speed was then increased to 46,025 *g* to monitor sedimentation of the unassociated fraction of the sample. The interference sedimentation velocity data initially were analyzed using the second moment method to obtain the weight-averaged sedimentation coefficient (s_{sm}). The second moment analysis yields s_{sm} for each scan, providing that the scan has a defined plateau and meniscus (Demeler, 2005). The s_{sm} was plotted against the scan number and linear region of the plot extrapolated to the *y*-axis to obtain the s_{sm} values reported in Figs 3 and 6. The scans also were analyzed by the time-derivative method to obtain the sedimentation coefficient distribution, g(s*) (Stafford, 1992). All sedimentation coefficients are expressed in Svedberg units (S); one Svedberg is equal to 10^{-13} s. All data editing and analyses were conducted using the UltraScanIII software (Demeler & Gorbet, in press).

SAXS

SAXS experiments were performed at SPring-8 using the BL45XU beamline. Following the approach of Langmore and Paulson (1983), the SAXS data in this paper are shown as plots of $\log(I \times S^2)$ versus $1/S$, obtained after subtracting buffer scattering. Here, I and $1/S$ are the average intensity and inverse of the scattering vector, respectively. $I \times S^2$ gives the true relative strength (power) of the structural periodicities in the samples (Langmore & Paulson, 1983). A peak in the X-ray scattering at a $1/S$ nm shows a periodicity of $1/S$ nm in the object. The data were averaged within concentric annuli of different radii about the experimental center to yield the average intensity I as a function of S.

BL45XU was set up for the SAXS experiment as follows (Fujisawa *et al*, 2000). The X-ray wavelength and sample-to-detector distances were 1.0 Å (12.4 keV) and 3.5 m. While Nishino *et al* (2012) (Fig 3C) and Joti *et al* (2012) (Fig 3C) performed SAXS with a rather large angle setting, covering from ~2 to ~80 nm, in the present work we took a smaller angle setting from ~5 nm to > 100 nm to fully cover the 30- to 40-nm range. The sample cell is made of stainless steel with 3 mm thickness sealed by 0.02-mm-thick synthetic quarts windows. The sample volume of it is 25 μl. The chromatin solutions and nuclei suspension were exposed to the X-ray beam. Scattering data for the chromatin samples and buffer were collected at room temperature using an imaging plate system (R-AXIS IV++; Rigaku) or 2D photon counting detector (PILATUS3X 2M; Dectris). Native chicken chromatin (Fig 7C and D) was purified as described in Ura and Kaneda (2001) with minor modifications. The HeLa nuclei used did not contain ribosomes.

Micrococcal nuclease digestion

Four micrograms of 601 nucleosome arrays was incubated in H10Mg5+Ca buffer [10 mM HEPES–KOH (pH 7.4), 0.15 mM $CaCl_2$, 0.1 mM PMSF, and 5 mM $MgCl_2$] to form the oligomers. For MNase digestion, the oligomers were digested for 5 min at 37°C using 1.6 U of MNase per μg of DNA. The reaction was stopped with 1 mM EGTA. The samples were subjected to fluorescence microscopy (FM) imaging or the differential centrifugation assay (9,100 *g* for 5 min). For FM imaging, the samples were spun onto BSA-coated coverslips and processed as described for the nuclei imaging. For the verification of complete MNase digestion, DNA was purified, electrophoresed on 1.2% agarose gel, and visualized by staining with ethidium bromide.

Computer modeling

We constructed model structures for a dinucleosome (PDB code: 1kx5), one-start and two-start 30-nm chromatin fiber models with 12-mer nucleosomes, and simulated oligomers containing tightly packed 30-nm chromatin fiber models. The 12-mer nucleosome models for the one-start and the two-start helixes were constructed based on the atomic coordinate models with 22-mer nucleosomes, which were kindly provided by Dr. D. Rhodes, LMB, UK (Schalch *et al*, 2005; Robinson & Rhodes, 2006). The simulated oligomers were modeled as follows: (i) The position and orientation of the first 12-mer (one-start helix or two-start helix) were generated randomly within a sphere with the radius *R* (Appendix Table S1). (ii) The position and orientation of the second 12-mer were generated randomly within a sphere with the radius *R* (Appendix Table S1), so that the two 12-mers have a contact. Here, two 12-mers are defined to have a contact if the distance between closest nucleosomes of the two 12-mers is < 12 nm. Selection of the model (one-start or two-start) was done using the random number. (iii) The position and orientation of the third and later 12-mers were generated randomly within a sphere with the radius R (Appendix Table S1), so that the 12-mer has at least two contacts with the previous 12-mers.

In the computation of SAXS profiles for the simulated oligomers, we generated three kinds of simulated oligomers containing 13, 42, and 100 of the 12-mer. SAXS profiles of 10 structures of each simulated oligomer were calculated and their average was obtained. Appendix Table S1 summarizes the parameters used in the modeling of the oligomeric structures.

SAXS profiles of the constructed model structures were calculated using the following equation:

$$I(S) = \sum_{i,j} f_i(S) f_j(S) \frac{\sin(2\pi S r_{ij})}{2\pi S r_{ij}},$$

where $f_i(S)$ and r_{ij} are the form factor of the *i*-th atom and the distance between *i*-th and *j*-th atoms, respectively. Here, the summation is over non-hydrogen atoms in each model. Software of our own making, which is parallelized using a message passing interface (MPI) library, was adopted to compute SAXS profiles for a few tens of millions of atoms efficiently. On request, the source file and model file are available.

Expanded View for this article is available online.

Acknowledgements
We thank Dr. S. Hihara for the technical assistance, Dr. J.J. Hayes for his critical reading of this manuscript, and Dr. M. Yamamoto for his support at SPring-8 BL45XU. This work was supported by JST CREST Grant and MEXT Grant 23115005 (to K.M.) and NIH Grant GM045916 (to J.H.). Part of the computation was performed using the "Thin compute nodes" in the NIG supercomputer system. The synchrotron radiation experiments were performed at BL45XU in SPring-8 with the approval of RIKEN (Proposal No. 20120023, 20130016, 20140025, 20150079).

Author contributions
KM and JCH designed the project; RR and ES synthesized the 12-mer nucleosome arrays and oligomers; RR analyzed them by TEM and analytical ultracentrifugation; ST, KM, RR, and JH performed FM imaging of the oligomers and MNase digestion; KM, ST, CK, HS, and JD prepared human nuclei and chromatin and performed FM imaging; KM, TH, YJ, and TI performed SAXS analysis; JCH and KM wrote the manuscript with input from all other authors.

Conflict of interest
The authors declare that they have no conflict of interest.

References

Alberts B, Johnson A, Lewis J, Raff M, Roberts K, Walter P (2007) *Molecular Biology of the Cell*, 5th edn. New York: Garland Science

Albiez H, Cremer M, Tiberi C, Vecchio L, Schermelleh L, Dittrich S, Kupper K, Joffe B, Thormeyer T, von Hase J, Yang S, Rohr K, Leonhardt H, Solovei I, Cremer C, Fakan S, Cremer T (2006) Chromatin domains and the interchromatin compartment form structurally defined and functionally interacting nuclear networks. *Chromosome Res* 14: 707 – 733

Barbieri M, Fraser J, Lavitas LM, Chotalia M, Dostie J, Pombo A, Nicodemi M (2014) A polymer model explains the complexity of large-scale chromatin folding. *Nucleus* 4: 267 – 273

Bouchet-Marquis C, Dubochet J, Fakan S (2006) Cryoelectron microscopy of vitrified sections: a new challenge for the analysis of functional nuclear architecture. *Histochem Cell Biol* 125: 43 – 51

Carruthers LM, Bednar J, Woodcock CL, Hansen JC (1998) Linker histones stabilize the intrinsic salt-dependent folding of nucleosomal arrays:

mechanistic ramifications for higher-order chromatin folding. *Biochemistry* 37: 14776 – 14787

Carruthers LM, Hansen JC (2000) The core histone N termini function independently of linker histones during chromatin condensation. *J Biol Chem* 275: 37285 – 37290

Cremer T, Cremer M (2010) Chromosome territories. *Cold Spring Harb Perspect Biol* 2: a003889

Dekker J, Marti-Renom MA, Mirny LA (2013) Exploring the three-dimensional organization of genomes: interpreting chromatin interaction data. *Nat Rev Genet* 14: 390 – 403

Demeler B, van Holde KE (2004) Sedimentation velocity analysis of highly heterogeneous systems. *Anal Biochem* 335: 279 – 288

Demeler B (2005) UltraScan – a comprehensive data analysis software package for analytical ultracentrifugation experiments. In *Modern Analytical Ultracentrifugation: Techniques and Methods*, Scott DJ, Harding SE, Rowe AJ (eds), pp 210 – 230. London: Royal Society of Chemistry

Demeler B, Gorbet GE (in press) Analytical ultracentrifugation data analysis with ultrascan-III. In *Analytical Ultracentrifugation: Instrumentation, Software, and Applications*, Uchiyama S, Stafford WF, Laue T (eds), Chapter 8. Japan: Springer

Dhall A, Wei S, Fierz B, Woodcock CL, Lee TH, Chatterjee C (2014) Sumoylated human histone H4 prevents chromatin compaction by inhibiting long-range internucleosomal interactions. *J Biol Chem* 289: 33827 – 33837

Dixon JR, Selvaraj S, Yue F, Kim A, Li Y, Shen Y, Hu M, Liu JS, Ren B (2012) Topological domains in mammalian genomes identified by analysis of chromatin interactions. *Nature* 485: 376 – 380

Doniach S (2001) Changes in biomolecular conformation seen by small angle X-ray scattering. *Chem Rev* 101: 1763 – 1778

Dorigo B, Schalch T, Bystricky K, Richmond TJ (2003) Chromatin fiber folding: requirement for the histone H4 N-terminal tail. *J Mol Biol* 327: 85 – 96

Dorigo B, Schalch T, Kulangara A, Duda S, Schroeder RR, Richmond TJ (2004) Nucleosome arrays reveal the two-start organization of the chromatin fiber. *Science* 306: 1571 – 1573

Dubin SB, Benedek GB, Bancroft FC, Freifelder D (1970) Molecular weights of coliphages and coliphage DNA. II. Measurement of diffusion coefficients using optical mixing spectroscopy, and measurement of sedimentation coefficients. *J Mol Biol* 54: 547 – 556

Eagen KP, Hartl TA, Kornberg RD (2015) Stable chromosome condensation revealed by chromosome conformation capture. *Cell* 163: 934 – 946

Earnshaw WC, Laemmli UK (1983) Architecture of metaphase chromosomes and chromosome scaffolds. *J Cell Biol* 96: 84 – 93

Eltsov M, Maclellan KM, Maeshima K, Frangakis AS, Dubochet J (2008) Analysis of cryo-electron microscopy images does not support the existence of 30-nm chromatin fibers in mitotic chromosomes *in situ*. *Proc Natl Acad Sci USA* 105: 19732 – 19737

Fan JY, Gordon F, Luger K, Hansen JC, Tremethick DJ (2002) The essential histone variant H2A.Z regulates the equilibrium between different chromatin conformational states. *Nat Struct Biol* 9: 172 – 176

Fan Y, Nikitina T, Zhao J, Fleury TJ, Bhattacharyya R, Bouhassira EE, Stein A, Woodcock CL, Skoultchi AI (2005) Histone H1 depletion in mammals alters global chromatin structure but causes specific changes in gene regulation. *Cell* 123: 1199 – 1212

Fierz B, Chatterjee C, McGinty RK, Bar-Dagan M, Raleigh DP, Muir TW (2011) Histone H2B ubiquitylation disrupts local and higher-order chromatin compaction. *Nat Chem Biol* 7: 113 – 119

Finch JT, Klug A (1976) Solenoidal model for superstructure in chromatin. *Proc Natl Acad Sci USA* 73: 1897 – 1901

Fujisawa T, Inoue K, Oka T, Iwamoto H, Uruga T, Kumasaka T, Inoko Y, Yagi N, Yamamoto M, Ueki T (2000) Small-angle X-ray scattering station at the SPring-8 RIKEN beamline. *J Appl Cryst* 33: 797 – 800

Fussner E, Strauss M, Djuric U, Li R, Ahmed K, Hart M, Ellis J, Bazett-Jones DP (2012) Open and closed domains in the mouse genome are configured as 10-nm chromatin fibres. *EMBO Rep* 13: 992 – 996

Gan L, Ladinsky MS, Jensen GJ (2013) Chromatin in a marine picoeukaryote is a disordered assemblage of nucleosomes. *Chromosoma* 122: 377 – 386

Gilbert N, Boyle S, Fiegler H, Woodfine K, Carter NP, Bickmore WA (2004) Chromatin architecture of the human genome: gene-rich domains are enriched in open chromatin fibers. *Cell* 118: 555 – 566

Gordon F, Luger K, Hansen JC (2005) The core histone N-terminal tail domains function independently and additively during salt-dependent oligomerization of nucleosomal arrays. *J Biol Chem* 280: 33701 – 33706

Grigoryev SA, Arya G, Correll S, Woodcock CL, Schlick T (2009) Evidence for heteromorphic chromatin fibers from analysis of nucleosome interactions. *Proc Natl Acad Sci USA* 106: 13317 – 13322

Grigoryev SA, Woodcock CL (2012) Chromatin organization – the 30 nm fiber. *Exp Cell Res* 318: 1448 – 1455

Hansen JC, Lohr D (1993) Assembly and structural properties of subsaturated chromatin arrays. *J Biol Chem* 268: 5840 – 5848

Hansen JC (2002) Conformational dynamics of the chromatin fiber in solution: determinants, mechanisms, and functions. *Annu Rev Biophys Biomol Struct* 31: 361 – 392

Hashimoto H, Takami Y, Sonoda E, Iwasaki T, Iwano H, Tachibana M, Takeda S, Nakayama T, Kimura H, Shinkai Y (2010) Histone H1 null vertebrate cells exhibit altered nucleosome architecture. *Nucleic Acids Res* 38: 3533 – 3545

Hihara S, Pack CG, Kaizu K, Tani T, Hanafusa T, Nozaki T, Takemoto S, Yoshimi T, Yokota H, Imamoto N, Sako Y, Kinjo M, Takahashi K, Nagai T, Maeshima K (2012) Local nucleosome dynamics facilitate chromatin accessibility in living mammalian cells. *Cell Rep* 2: 1645 – 1656

Hirano T (2015) Chromosome dynamics during mitosis. *Cold Spring Harb Perspect Biol* 7: a015792

Hudson DF, Vagnarelli P, Gassmann R, Earnshaw WC (2003) Condensin is required for nonhistone protein assembly and structural integrity of vertebrate mitotic chromosomes. *Dev Cell* 5: 323 – 336

Jason LJ, Moore SC, Ausio J, Lindsey G (2001) Magnesium-dependent association and folding of oligonucleosomes reconstituted with ubiquitinated H2A. *J Biol Chem* 276: 14597 – 14601

Joti Y, Hikima T, Nishino Y, Kamada F, Hihara S, Takata H, Ishikawa T, Maeshima K (2012) Chromosomes without a 30-nm chromatin fiber. *Nucleus* 3: 404 – 410

Kalashnikova AA, Porter-Goff ME, Muthurajan UM, Luger K, Hansen JC (2013) The role of the nucleosome acidic patch in modulating higher order chromatin structure. *J R Soc Interface* 10: 20121022

Kan PY, Caterino TL, Hayes JJ (2009) The H4 tail domain participates in intra- and internucleosome interactions with protein and DNA during folding and oligomerization of nucleosome arrays. *Mol Cell Biol* 29: 538 – 546

Kraulis PJ (1991) MOLSCRIPT: a program to produce both detailed and schematic plots of protein structures. *J Appl Cryst* 24: 946 – 950

Langmore JP, Paulson JR (1983) Low angle x-ray diffraction studies of chromatin structure *in vivo* and in isolated nuclei and metaphase chromosomes. *J Cell Biol* 96: 1120 – 1131

Li G, Zhu P (2015) Structure and organization of chromatin fiber in the nucleus. *FEBS Lett* 589: 2893 – 2904

Liu Y, Lu C, Yang Y, Fan Y, Yang R, Liu CF, Korolev N, Nordenskiold L (2011) Influence of histone tails and H4 tail acetylations on nucleosome-nucleosome interactions. *J Mol Biol* 414: 749 – 764

Lowary PT, Widom J (1998) New DNA sequence rules for high affinity binding to histone octamer and sequence-directed nucleosome positioning. *J Mol Biol* 276: 19 – 42

Lu X, Hamkalo B, Parseghian MH, Hansen JC (2009) Chromatin condensing functions of the linker histone C-terminal domain are mediated by specific amino acid composition and intrinsic protein disorder. *Biochemistry* 48: 164 – 172

Luger K, Mader AW, Richmond RK, Sargent DF, Richmond TJ (1997) Crystal structure of the nucleosome core particle at 2.8 A resolution. *Nature* 389: 251 – 260

MacRaild CA, Hatters DM, Lawrence LJ, Howlett GJ (2003) Sedimentation velocity analysis of flexible macromolecules: self-association and tangling of amyloid fibrils. *Biophys J* 84: 2562 – 2569

Maeshima K, Hihara S, Eltsov M (2010) Chromatin structure: does the 30-nm fibre exist *in vivo*? *Curr Opin Cell Biol* 22: 291 – 297

Maeshima K, Imai R, Hikima T, Joti Y (2014a) Chromatin structure revealed by X-ray scattering analysis and computational modeling. *Methods* 70: 154 – 161

Maeshima K, Imai R, Tamura S, Nozaki T (2014b) Chromatin as dynamic 10-nm fibers. *Chromosoma* 123: 225 – 237

McBryant SJ, Krause C, Woodcock CL, Hansen JC (2008) The silent information regulator 3 protein, SIR3p, binds to chromatin fibers and assembles a hypercondensed chromatin architecture in the presence of salt. *Mol Cell Biol* 28: 3563 – 3572

Muthurajan UM, McBryant SJ, Lu X, Hansen JC, Luger K (2011) The linker region of macroH2A promotes self-association of nucleosomal arrays. *J Biol Chem* 286: 23852 – 23864

Nikitina T, Shi X, Ghosh RP, Horowitz-Scherer RA, Hansen JC, Woodcock CL (2007) Multiple modes of interaction between the methylated DNA binding protein MeCP2 and chromatin. *Mol Cell Biol* 27: 864 – 877

Nishino Y, Eltsov M, Joti Y, Ito K, Takata H, Takahashi Y, Hihara S, Frangakis AS, Imamoto N, Ishikawa T, Maeshima K (2012) Human mitotic chromosomes consist predominantly of irregularly folded nucleosome fibres without a 30-nm chromatin structure. *EMBO J* 31: 1644 – 1653

Nora EP, Lajoie BR, Schulz EG, Giorgetti L, Okamoto I, Servant N, Piolot T, van Berlum N, Meisig J, Sedat JW, Gribnau J, Barillot E, BLüthgen N, Dekker J, Heard E (2012) Spatial partitioning of the regulatory landscape of the X-inactivation centre. *Nature* 485: 381 – 385

Ohta S, Wood L, Bukowski-Wills JC, Rappsilber J, Earnshaw WC (2010) Building mitotic chromosomes. *Curr Opin Cell Biol* 23: 114 – 121

Pepenella S, Murphy KJ, Hayes JJ (2014) Intra- and inter-nucleosome interactions of the core histone tail domains in higher-order chromatin structure. *Chromosoma* 123: 3 – 13

Rao SS, Huntley MH, Durand NC, Stamenova EK, Bochkov ID, Robinson JT, Sanborn AL, Machol I, Omer AD, Lander ES, Aiden EL (2014) A 3D map of the human genome at kilobase resolution reveals principles of chromatin looping. *Cell* 159: 1665 – 1680

Ricci MA, Manzo C, Garcia-Parajo MF, Lakadamyali M, Cosma MP (2015) Chromatin fibers are formed by heterogeneous groups of nucleosomes *in vivo*. *Cell* 160: 1145 – 1158

Robinson PJ, Fairall L, Huynh VA, Rhodes D (2006) EM measurements define the dimensions of the "30-nm" chromatin fiber: evidence for a compact, interdigitated structure. *Proc Natl Acad Sci USA* 103: 6506 – 6511

Robinson PJ, Rhodes D (2006) Structure of the "30 nm" chromatin fibre: a key role for the linker histone. *Curr Opin Struct Biol* 16: 336 – 343

Roe R-J (2000) *Methods of X-Ray and Neutron Scattering in Polymer Science*. New York, USA: Oxford University Press

Rogge RA, Kalashnikova AA, Muthurajan UM, Porter-Goff ME, Luger K, Hansen JC (2013) Assembly of nucleosomal arrays from recombinant core histones and nucleosome positioning DNA. *J Vis Exp* 79: e50354

Rogge RA, Hansen JC (2015) Sedimentation velocity analysis of large oligomeric chromatin complexes using interference detection. *Methods Enzymol* 562: 349 – 362

Schalch T, Duda S, Sargent DF, Richmond TJ (2005) X-ray structure of a tetra-nucleosome and its implications for the chromatin fibre. *Nature* 436: 138 – 141

Schuck P (2013) Analytical ultracentrifugation as a tool for studying protein interactions. *Biophys Rev* 5: 159 – 171

Schwarz PM, Hansen JC (1994) Formation and stability of higher order chromatin structures. Contributions of the histone octamer. *J Biol Chem* 269: 16284 – 16289

Schwarz PM, Felthauser A, Fletcher TM, Hansen JC (1996) Reversible oligonucleosome self-association: dependence on divalent cations and core histone tail domains. *Biochemistry* 35: 4009 – 4015

Sexton T, Yaffe E, Kenigsberg E, Bantignies F, Leblanc B, Hoichman M, Parrinello H, Tanay A, Cavalli G (2012) Three-dimensional folding and functional organization principles of the drosophila genome. *Cell* 148: 458 – 472

Shogren-Knaak M, Ishii H, Sun JM, Pazin MJ, Davie JR, Peterson CL (2006) Histone H4-K16 acetylation controls chromatin structure and protein interactions. *Science* 311: 844 – 847

Simpson RT, Thoma F, Brubaker JM (1985) Chromatin reconstituted from tandemly repeated cloned DNA fragments and core histones: a model system for study of higher order structure. *Cell* 42: 799 – 808

Song F, Chen P, Sun D, Wang M, Dong L, Liang D, Xu RM, Zhu P, Li G (2014) Cryo-EM study of the chromatin fiber reveals a double helix twisted by tetranucleosomal units. *Science* 344: 376 – 380

Stafford WF III (1992) Boundary analysis in sedimentation transport experiments: a procedure for obtaining sedimentation coefficient distributions using the time derivative of the concentration profile. *Anal Biochem* 203: 295 – 301

Szerlong HJ, Prenni JE, Nyborg JK, Hansen JC (2010) Activator-dependent p300 acetylation of chromatin *in vitro*: enhancement of transcription by disruption of repressive nucleosome-nucleosome interactions. *J Biol Chem* 285: 31954 – 31964

Takata H, Hanafusa T, Mori T, Shimura M, Iida Y, Ishikawa K, Yoshikawa K, Yoshikawa Y, Maeshima K (2013) Chromatin compaction protects genomic DNA from radiation damage. *PLoS ONE* 8: e75622

Talbert PB, Ahmad K, Almouzni G, Ausio J, Berger F, Bhalla PL, Bonner WM, Cande WZ, Chadwick BP, Chan SW, Cross GA, Cui L, Dimitrov SI, Doenecke D, Eirin-Lopez JM, Gorovsky MA, Hake SB, Hamkalo BA, Holec S, Jacobsen SE *et al* (2012) A unified phylogeny-based nomenclature for histone variants. *Epigenetics Chromatin* 5: 7

Tse C, Hansen JC (1997) Hybrid trypsinized nucleosomal arrays: identification of multiple functional roles of the H2A/H2B and H3/H4 N-termini in chromatin fiber compaction. *Biochemistry* 36: 11381 – 11388

Ura K, Kaneda Y (2001) Reconstitution of chromatin *in vitro*. *Methods Mol Biol* 181: 309 – 325

Valouev A, Johnson SM, Boyd SD, Smith CL, Fire AZ, Sidow A (2011) Determinants of nucleosome organization in primary human cells. *Nature* 474: 516 – 520

Visvanathan A, Ahmed K, Even-Faitelson L, Lleres D, Bazett-Jones DP, Lamond AI (2013) Modulation of higher order chromatin conformation in

mammalian cell nuclei can be mediated by polyamines and divalent cations. *PLoS ONE* 8: e67689

Widom J, Klug A (1985) Structure of the 300A chromatin filament: X-ray diffraction from oriented samples. *Cell* 43: 207 – 213

Woodcock CL, Frado LL, Rattner JB (1984) The higher-order structure of chromatin: evidence for a helical ribbon arrangement. *J Cell Biol* 99: 42 – 52

Woodcock CL, Woodcock H, Horowitz RA (1991) Ultrastructure of chromatin. I. Negative staining of isolated fibers. *J Cell Sci* 99(Pt 1): 99 – 106

Woodcock CL, Skoultchi AI, Fan Y (2006) Role of linker histone in chromatin structure and function: H1 stoichiometry and nucleosome repeat length. *Chromosome Res* 14: 17 – 25

Zheng C, Lu X, Hansen JC, Hayes JJ (2005) Salt-dependent intra- and internucleosomal interactions of the H3 tail domain in a model oligonucleosomal array. *J Biol Chem* 280: 33552 – 33557

